Micro/Nanoscale Thermometry for Cellular Thermal Sensing

*Tingting Bai and Ning Gu**

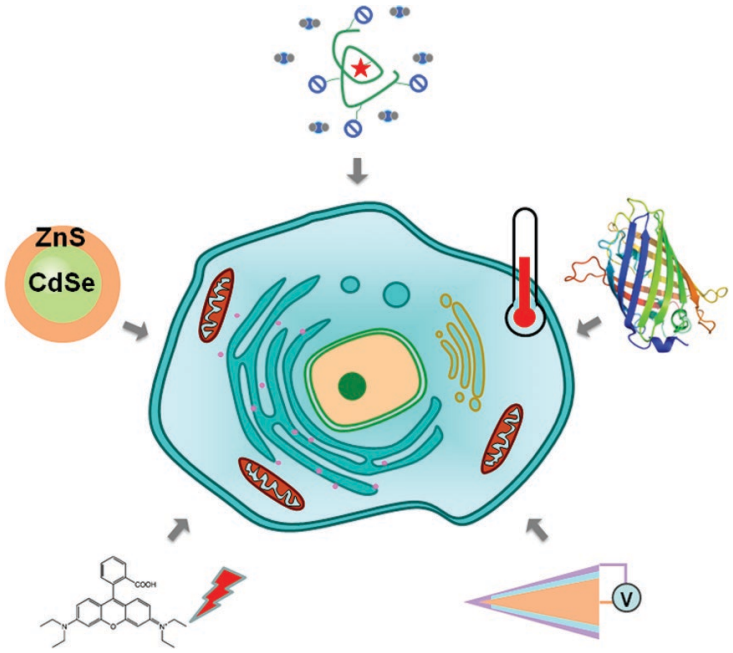

From the Contents

Temperature is a key parameter to regulate cell function, and biochemical reactions inside a cell in turn affect the intracellular temperature. It's vitally necessary to measure cellular temperature to provide sufficient information to fully understand life science, while the conventional methods are incompetent. Over the last decade, many ingenious thermometers have been developed with the help of nanotechnology, and real-time intracellular temperature measurement at the micro/nanoscale has been realized with high temporal-spatial resolution. With the help of these techniques, several mechanisms of thermogenesis inside cells have been investigated, even in subcellular organelles. Here, current developments in cellular thermometers are highlighted, and a picture of their applications in cell biology is presented. In particular, temperature measurement principle, thermometer design and latest achievements are also introduced. Finally, the existing opportunities and challenges in this ongoing field are discussed.

DOI: 10.1002/smll.201600665

1. Introduction

Temperature is probably the most important and fundamental parameter for cellular activities.[1–3] As the basic unit of living organisms, cells appear as sacs of fluid surrounded by membranes (and rigid walls for plant cells). The fluid inside of each single cell contains floating chemicals and organelles. Taking eukaryotic cells for example, the organelles are the compartments created by intracellular membrane and have different functions.[4–8] The nucleus is a place mainly containing and synthesizing DNA.[9] Endoplasmic reticulum is responsible for protein synthesis in a cell.[10] Mitochondria (and chloroplast in plant) is the power house of the cell, which stores and releases the energy in the form of a small molecule called adenosine triphosphate (ATP).[11] Temperature variation at the single-cell level happens all the time due to the many biochemical reactions inside the cell. It can be divided into two categories: the change caused by cell activities and the response to external stimuli.[12] On the one hand, it is known that every cell activities, such as division, gene expression, enzyme reaction, metabolism and pathological state, is accompanied by temperature changes.[5,6,13–15] Cancer cells have higher temperatures than those of normal tissues because of their enhanced metabolic activity, which has been proved by a clinical experiment.[16,17] On the other hand, cellular thermal sensing will be beneficial to understand the influence of external environment to cells. For example, in the field of hyperthermia therapy, tumor cells are killed by heating at temperatures above 40 °C.[18–21] Without the exact monitoring of the heating procedure, the health tissues around tumors would also be damaged. Consequently, temperature sensing of living cells would provide not only insight into a variety of cell events, but also a grasp of cellular pathological state, permitting the development of diagnostic and therapeutic techniques for some diseases.

Some early reports used the conventional thermometers to detect temperature changes of cell groups. The microcalorimeter is the earliest method for direct cellular thermosensing.[22] It has been used to monitor heat production property of various cell types such as erythrocyte, hepatocytes, lymphocytes, thrombocytes, muscle cells and adipocytes.[23–27] However the readout is only an overall outcome of the cells in the measuring cup, while 10^4–10^5 cells are sufficient for one measurement.[28] So the spatial and temporal resolution is very poor. Infrared thermography is another option for temperature measurement, which has been widely applied in researching and industrial field due to its non-contact, non-destructive and high-throughput properties.[16,29,30] Paulik et al. used the infrared thermography to measure real-time thermogenesis of isolated cells for the first time.[30] The intracellular temperature changes unpredictably and non-uniformly during different cellular activities, owing to the nonhomogeneity of cytoplasm.[13,15] However, the spatial resolution of infrared thermography is only ≈10 um and the precision depends on the properties of the object studied.[31,32] It can only be used to detect surface temperatures of objects and does not yield absolute temperature values so a correct calibration is prerequisite for all measurements.[31] Moreover, infrared radiation does not penetrate glass and water.[31] So to sum up, the conventional infrared thermometer cannot be used for the accurate intracellular thermosensing of living cells in the culture medium.

Apart from the conventional methods, living cell thermosensing is in urgent need of precise thermometers working at the micro/nanoscale with high spatial resolution. Brites et al. have offered a general overview on many kinds of nanothermometers.[32] Among these methods, only some examples can be used to measure temperature in living cells. After that, Jaque et al. and Uchiyama et al. reviewed various kinds of fluorescent nanothermometers for intracellular thermal sensing.[4,33] With the development of nanotechnology in recent years, the investigation of cellular thermometers has been largely explored, and many new and effective approaches have emerged currently. On this basis, this review presents an overview of these developments of technique and their applications in cell biology. The methods are categorized according to the sensing principle and listed in **Table 1**, which is replenished and modified on the basis of former reports, including organic fluorophores, rare-earth metal complex, quantum dots, inorganic materials, thermoresponsive synthetic polymers, biomolecules, thermocouples, and some composite structures.[4–7] Based on the reception mode of signal, they can also be divided into the non-contact (luminescent) and contact thermometer. In addition, the applications of these thermometers in biological tissues are also included in Table 1. Some features or parameters of these thermometers are critical for measuring and need to be defined first in this review.[31] The temperature range means the range from the lowest to the highest temperature that can be measured by a method. The temperature resolution indicates the minimum detectable temperature signal. Both of them are expressed in °C. The relative sensitivity (S) of these techniques discussed in this review and commonly used in previous studies is defined as:[4,32,34]

$$S = \frac{\left(\frac{\partial Q}{\partial T}\right)}{Q} \tag{1}$$

where Q is an experimental parameter corresponding with temperature (T). The S is usually expressed as percent change per degree Celsius ([%/°C]). To precisely observe intracellular temperature distribution, the thermometers should simultaneously satisfy many requirements: proper detection range; high temperature resolution; high spatial resolution; real-time capability; functional independence from environmental changes in pH, ionic strength, and surrounding biomacromolecules; a concentration-independent output,

Dr. T. T. Bai, Prof. N. Gu
State Key Laboratory of Bioelectronics
Jiangsu Key Laboratory for Biomaterials and Devices
School of Biological Science and Medical Engineering
Southeast University
Nanjing 210096, P. R. China
E-mail: guning@seu.edu.cn

DOI: 10.1002/smll.201600665

high repeatability and user-friendly operation.[6,7] Here, we will discuss the advantages and drawbacks of these cellular thermometers mainly from these aspects, and summarize the achievements and obstacles of this challenging and multidisciplinary field.

2. Luminescence-Based Thermometry

Optical imaging methods for cells have been broadly applied in life, research and industry fields due to its non-contact, non-invasive characteristics. Luminescent thermometers combined with existing and mature imaging techniques make the operation feasible. They can work remotely with high temperature resolution, spatial resolution and fast data acquisition, and are very applicable to biological samples in fluids. Almost simultaneously, Brites et al. and Jaque et al. separately presented two early and complete summaries of luminescence nanothermometry in 2012, when the thermometry of living cells were just getting started.[32,33] They introduced and compared the different classes of luminescence nanothermometry from many aspects, such as principle, resolution, advantages and disadvantages. The temperature determination by luminescence mostly depends on the fluorescence intensity, the maximum emission wavelength and the decay of lifetime changes, which are caused by the temperature-dependent structure changes of luminescent probes. Because of some limitations on stability, accuracy and practicality, only a few of these luminescence nanothermometers had been used in the temperature measurement of living cells, and provided some plain results. In recent years, numerous luminescence techniques for thermal imaging of living cells have sprung up. The most relevant and important ones are reviewed and compared in this section from many aspects.

2.1. Organic Fluorophores

Organic fluorophores were first mentioned as "temperature indicators" in a patent of 1941.[79] They exhibit a temperature-dependent property: when the temperature increases, the intensity of excited fluorescence decreases and the peak shifts to longer wavelength.[80] Up to now, there are a lot kinds of fluorescent dyes commercially available with different characteristics to meet the experimental requirements. Any kinds of thermometers using fluorescent dyes can be easily designed, and has provided a leading performance in many fields at the micro/nanoscale.[35–40,79] Chapman et al. first showed that two fluorescent membrane probes NBD-PC (2-(12-NBD-amino) dodecanoyl-1-hexadecanoyl-sn-glycero-3-phosphocholin) and laurdan (6-dodecanoyl-2-dimethylaminonaphthalene) can be used as sensitive optical thermometers in living cell.[35] NBD-conjugated lipids insert into the plasma membrane of Chinese hamster ovary (CHO) cells after the incubation of cells in a culture medium containing NBD-PC. The fluorescence decreases with the increasing medium temperature, and provides a reasonable temperature resolution (approximately 2 °C). In contrast, the fluorescence of laurdan located on the cell membrane changes as the membrane undergoes a gel-to-liquid-crystalline phase, which depends on the temperature. The microenvironmental sensitivity of laurdan permits better temperature resolution (0.1–1 °C) at the expense of a more limited dynamic range.

DyLight549 is another organic fluorophore that has been used to measure the surface temperature of the superparamagnetic $MnFe_2O_4$ nanoparticles, which are targeted to ion channel on the cellular membrane.[36] DyLight549 conjugated to the nanoparticle by biotin-streptavidin linkage. The emission intensity of DyLight549 decreased after the heating of $MnFe_2O_4$ nanoparticles under a radio frequency magnetic field, indicating heating of more than 15 °C within 15 s (**Figure 1**).

Apart from the cytomembrane thermal sensing, small-molecule fluorescent thermometers have been reported to sensing at subcellular level, selectively targeting the organelles.[37–40] Among many organelles, the mitochondrion is a well-known heat producing organelle. Arai et al. screened many rosamine compounds for monitoring temperature changes in mitochondria with high temperature sensitivity.[39] After screening, the best compound named Mito thermo yellow was used as a mitochondrial specific dye. The fluorescence intensity of Mito thermo yellow in living NIH3T3 cells declined rapidly when the temperature of the extracellular medium increased, giving a temperature sensitivity of 2.7%/°C. In other cells, the temperature sensitivities changed from 2.0 to 2.8%/°C, which is possible due to the chemical environment differences in mitochondria. Another group designed a mitochondria-targeting ratiometric temperature probe (Mito-RTP), which is composed of two kinds of dyes:

Tingting Bai joined the group of Prof. Gu during her B.S. research project on the assembly of gold nanoparticles for biomedical detection. She received her bachelor's degree in Biomedical Engineering from Southeast University, and is currently continuing her Ph.D. studies under the supervision of Prof. Gu. Her research interests include the preparation of gold/silver bimetallic nanoparticles for the detection biomolecules, and the development of micro-thermocouples for intracellular temperature measurement.

Ning Gu completed his Ph.D. studies in Biomedical Engineering at the Southeast University in 1996, and then went to Tokyo University as a visiting scholar. He was promoted as a full-time professor of Southeast University in 1997. He went to Yamanashi University, National Institute of Materials, Chemical Research (NIMS) with a postdoc fellowship (1998–1999), and the Institute for Molecular Science (IMS) as a visiting professor (2002). His current research interests include functional nanomaterials, nanofabrication, nanodevices, and the corresponding applications in biomedicine.

Table 1. Different thermometers for thermal sensing and imaging of living cells and biological tissues.

Thermometer	Year	Temperature-dependent signal	Temperature range/ resolution [°C]	Sensitivity	Calibration (environmental sensitivity)	Reversibility	Cells/ biological tissues	Operational approach	Monitoring point	Refs
1. Organic fluorophores										
NBD	1995	FI or FL	17–50/2	NA	In cells (sensitive to intracellular environment)	Negative	CHO	Incubation, 4 °C, 4 h	Cell membrane	[35]
Laurdan	1995	FI Ratio	16–41/0.1–1.0	NA	In cells (sensitive to intracellular environment)	Negative	CHO	Incubation, 37 °C, 35 min	Cell membrane	[35]
DyLight 549	2010	FI	25–42	–1.5%/°C	In water (NA)	NA	HEK293	Incubation, room temperature, 1 min	Cell membrane	[36]
ER thermo yellow	2014	FI	32–37	–3.9%/°C	In cells (resistant to environmental changes)	Positive	HeLa	Incubation, 37 °C, 30 min	Endoplasmic reticulum	[37]
ER thermo yellow	2016	FL	23–40	–0.96– –1.04%/°C	In cells (sensitive to environmental changes)	Positive	HeLa, C2C12	Incubation, 37 °C, 30 min	Endoplasmic reticulum	[38]
Mito thermo yellow	2015	FI	37–42	–2.0– –2.8%/°C	In cells (sensitive to intracellular environment)	Positive	HeLa, NIH3T3, C2C12, mESC, Chang, BAT	Incubation, 37 °C, 15 min	Mitochondria	[39]
Mito-RTP	2015	FI Ratio	25–43	–2.65%/°C	In PBS (resistant to pH and ionic strength changes)	Positive	HeLa	Incubation, 37 °C, 30 min	Mitochondria	[40]
2. Rare-earth metal complex										
Eu-TTA	1998	FI	15–40	NA	In cells (sensitive to environmental changes)	Negative	CHO	Incubation, room temperature, 30 min	Cell membrane	[41]
Eu-TTA within micropipette	2007	FI	25–50	–2.74%/°C	In DMSO (resistant to pH and ionic strength changes)	Positive	HeLa	Contact controlled by micromanipulator	Local region of cell membrane	[42]
Eu-TTA@ polymer NPs	2012	FI	20–60/0.3	–2.2%/°C	In PBS (resistant to pH and ionic strength changes)	Positive	HeLa	Incubation, 37 °C, 1 h	Endosomes/ lysosomes	[43]
$Ru(bpy)_3^{2+}$ doped silica NPs	2014	FI	25–45	–1.26%/°C	In water (NA)	Positive	HepG2	Incubation, 37 °C, 24 h	Cell interior	[44]
3. Quantum dots										
CdSe-QDs	2010	EW	30–60	0.025%/°C	In PBS (NA)	Positive	HeLa	Incubation, 37 °C, 2 h	Dotted within a cell	[45,46]
QD655	2011	EW	–20–12	0.016%/°C	In PDMS (NA)	Positive	NIH3T3	Using Qtracker cell labeling kit, 37 °C, 1 h	Dotted within a cell	[47]
CdSe-QDs	2013	EW	30–60	0.016%/°C	In PBS (NA)	Positive	Jurkat cells	Incubation	Dotted within a cell	[48]
CdSeS/ZnS@ polymer	2015	FI	25–45/0.43	–1.55%/°C	In water (resistant to pH and ionic strength changes)	Positive	HepG2	Incubation, 37 °C, 2 h	Dotted within a cell	[49]
CdSe-QDs	2013	EW	30–60	0.015%/°C	In PBS (NA)	Positive	Mouse tissue	Injection	Local tissue	[21]
4. Other inorganic materials										
$NaYF_4$:Er^{3+}, Yb^{3+} NPs	2010	FI ratio	NA	NA	In water (NA)	Positive	HeLa	Incubation, 37 °C, 1.5 h	Dotted within a cell	[50]
Nd^{3+}:LaF_3 NPs	2013	FI ratio	10–60	0.1%/°C	In water (NA)	Positive	Phantom skin tissue	NA	Local tissue	[51]

small 2016,
DOI: 10.1002/smll.201600665

Table 1. Continued.

Thermometer	Year	Temperature-dependent signal	Temperature range/ resolution [°C]	Sensitivity	Calibration (environmental sensitivity)	Reversibility	Cells/ biological tissues	Operational approach	Monitoring point	Refs
$NaYF_4$:Er^{3+},Yb^{3+} NPs	2016	FI ratio	10–36	–1.6%/°C	In water (NA)	Positive	HeLa	Mixing	Surrounding of a cell	[52]
Au nanoclusters (AuNCs)	2013	FL	15–45/0.3–0.5	NA	In cells (sensitive to intracellular environment)	Positive	HeLa	Incubation, 37 °C, 2 h	Dotted within a cell	[53]
Nanodiamonds nitrogen-vacancy centers	2013	Spin states with microwave excitations	–200–327/0.044	NA	In air (NA)	Positive	WS1	Delivered by nanowire	Dotted within a cell	[54]
Cu nanoclusters (CuNCs)	2015	FI	15–80	NA	In water (NA)	Positive	MC3T3-E1	Incubation, 37 °C, 2 h	Cell interior	[55]
5. Thermoresponsive synthetic polymers										
NIPAM-DBD nanogel	2009	FI	27–33/0.29–0.50	NA	In cells (resistant to pH and ionic strength changes)	Positive	COS7	Microinjection	Dotted within a cell	[17]
P(S-alt-MAn)-*b*-PNIPAm-AMC	2012	FI	32–35	NA	In water (sensitive to pH changes)	Positive	MDCK	Incubation, 37 °C, 3 h	Dotted within a cell	[56]
NNPAM-DBD	2012	FL	29–39/0.18–0.58	NA	In cell extract (resistant to pH and ionic strength changes)	Negative	COS7, HeLa	Microinjection	Dotted within a cell	[57]
NNPAM-DBD cationic copolymer	2013	FL	15–35/0.09–0.78	NA	In cells (sensitive to intracellular environment)	Negative	Yeast, MOLT-4, HEK293T	Incubation, 25 °C, 10 min	Cytoplasm, cell wall	[58]
NNPAM-DBD cationic copolymer	2015	FL	28–38/0.05–0.54	NA	In cell extract (resistant to pH and ionic strength changes)	Negative	HeLa, COS7, NIH3T3	Incubation, 25 °C, 10 min	Whole cell: cytoplasm, nucleus	[59]
Fe_3O_4@SiO_2@(pNIPAM-co-RhBITC)/Au NPs	2015	FI	26–41	–4.84%/°C	In water (NA)	Positive	HeLa	Incubation, 37 °C, 2 h	Cell interior	[60]
6. Bio-molecules										
GFP	2012	FPA	20–60	–0.4%/°C	In PBS (sensitive to intracellular environment)	Positive	HeLa, U-87 MG	Genetically expressed	Whole cell	[61]
GFP	2013	FPA	20–60	–0.4%/°C	In PBS (sensitive to intracellular environment)	Positive	*C. elegans* neurons	Genetically expressed	Whole cell	[12]
tsGFPs	2013	FI ratio	34–41	NA	In cells (resistant to pH and ionic strength changes)	Positive	HeLa, brown adipocyte, skeletal muscle myotube	Genetically expressed	Cytoplasm, mitochondria, endoplasmic reticulum	[62]
L-MB	2012	FI	20–55/0.7	NA	In PBS (resistant to pH and ionic strength changes)	Positive	HeLa	Transfection	Nucleus	[63]
7. Non-luminescent thermometer										
Pt-W thermocouple	2011	Thermoelectric voltage	0–90/0.1	NA	In water (NA)	Positive	U251	Puncture controlled by micromanipulator	Local region within cell	[64]
Micropipette thermocouple	2011	Thermoelectric voltage	25–39	18%/°C	In water (NA)	Positive	RPE cells	Puncture controlled by micromanipulator	Local region within cell	[65]
Micropipette thermocouple	2013	Thermoelectric voltage	NA	4.0%/°C	In water (NA)	Positive	Leaves of *S. variegata* and *F. aurantiaca*	Puncture controlled by micromanipulator	Local region within cell	[66]

DOI: 10.1002/smll.201600665

Table 1. Continued.

Thermometer	Year	Temperature-dependent signal	Temperature range/ resolution [°C]	Sensitivity	Calibration (environmental sensitivity)	Reversibility	Cells/ biological tissues	Operational approach	Monitoring point	Refs
Nano-needle	2014	Resistance	24–60/0.01	NA	In water (NA)	Positive	NA	Micro-fluidic channel	Local region within cell	[67]
8. Composite Structures										
Pluronic P85-TRITC-HMA micelles	2011	FI ratio	20–30	NA	In water (NA)	NA	HeLa	Incubation, 37 °C, 3 h	Dotted within a cell	[68]
QD–QRs appended by Alexa-647	2012	FI ratio	20–40/0.1	2.4%/°C	In cells (sensitive to intracellular environment)	Positive	HeLa, NIH3T3	Assisted by cationic polymer colloid	Cell interior	[69]
PNIPAm-co-NBDAA/ PNIPAm-co-RhBAM	2014	FI ratio	34–40/0.3–0.5	NA	In cells (resistant to pH and ionic strength changes)	NA	HeLa	Incubation, 28 °C, 3 h	Dotted within a cell	[70]
Eu-TTA & rhodamine101@ polymer NPs	2014	FI ratio	26–40	–0.108 /°C	In solutions (resistant to pH and ionic strength changes)	Positive	HeLa	Incubation, 37 °C, 2 h	Dotted within a cell	[71]
Magnetic NPs@ Eu^{3+}/Tb^{3+} complexes@ P4VP@P(PEGA)	2015	FI ratio	22–42	5.8%/°C	In water (NA)	Positive	Opossum kidney (OK) cells	Incubation, 37 °C, 24 h	Around the nucleus	[72]
$(EuDT/Ir(ppy)_3$/ PS-MA)@PVA	2015	FI ratio	25–46	–4.0%/°C	In PBS (sensitive to environmental changes)	Positive	Fruit fly larva	Feeding	Remain in the guts	[73]
$NaGdF_4:Nd^{3+}$ NPs & QDs @ PLGA	2015	FI ratio	10–50	0.025/°C	In PBS (NA)	Positive	Chicken breast tissue	NA	NA	[74]
PNIPAM-DPTB-Nile Red nanogel	2015	FI ratio	34–56/0.2	NA	In water (NA)	Positive	NIH3T3	Incubation, 37 °C, 30 min	Cell interior	[75]
NNPAM-APTMA-DBThD-BODIPY	2015	FI ratio	25–44/0.01–0.25	NA	In solutions (resistant to pH and ionic strength changes)	Positive	MOLT-4, HEK293T	Incubation, 25 °C, 10 min	Whole cell: cytoplasm, nucleus	[76]
P(NIPAm-NBD-NSVB)- TfAuNCs	2015	FI ratio	31.8–38.5/0.3–0.5	NA	In cells (sensitive to intracellular environment)	Positive	HeLa	Incubation, 25 °C, 20 min	Cell interior	[77]
PEG-*b*-P(NIPAM-*co*-CMA), PEG-*b*-P(NIPAM-*co*-NBDAE), PEG-*b*-P(NIPAM-*co*-RhBEA)	2015	FI ratio	20–44	NA	In cell extract (NA)	Positive	HeLa	Incubation, 37 °C, 40 min	Cell interior	[78]

FI: fluorescence intensity; FL: fluorescence lifetime; EW: maximum emission wavelength; FPA: fluorescence polarization anisotropy; PBS: phosphate-buffered saline solution; NA: not available.

rhodamine B and CS NIR dye (**Figure 2**a).[40] From 25 to 43 °C, the fluorescence intensity of rhodamine B reversibly responded to temperature changes, whereas that of CS NIR dye was constant. The fluorescence intensity ratio of these two dyes showed a linear decline with increasing temperature (Figure 2b), giving a temperature sensitivity of –2.65%/°C. This ratiometric thermometer is insensitive to environmental parameters change, such as pH and ionic strength variation. Except mitochondrion, the sarco/endoplasmic reticulum (SR/ER) has also received attention as one of the organelles responsible for heat production recently.[81] Arai et al. reported a small organic molecule fluorescent thermometer (ER thermo yellow) with targeting ability to ER and high thermosensitivity (Figure 2d).[37,38] The fluorescence intensity decreased linearly with the increasing temperature, providing a high sensitivity of 3.9%/°C.[37] Furthermore, they used fluorescence lifetime imaging microscopy (FLIM) to image the temperature changes of myotubes, since the fluorescence lifetime of ER thermo yellow reduced with increasing temperature (Figure 2e).[38]

2.2. Rare-Earth Metal Complex

Europium (III) thenoyltrifluoro-acetonate (Eu-TTA) is a rare-earth chelate, whose emission intensity decreases rapidly

small 2016,
DOI: 10.1002/smll.201600665

small NANO MICRO

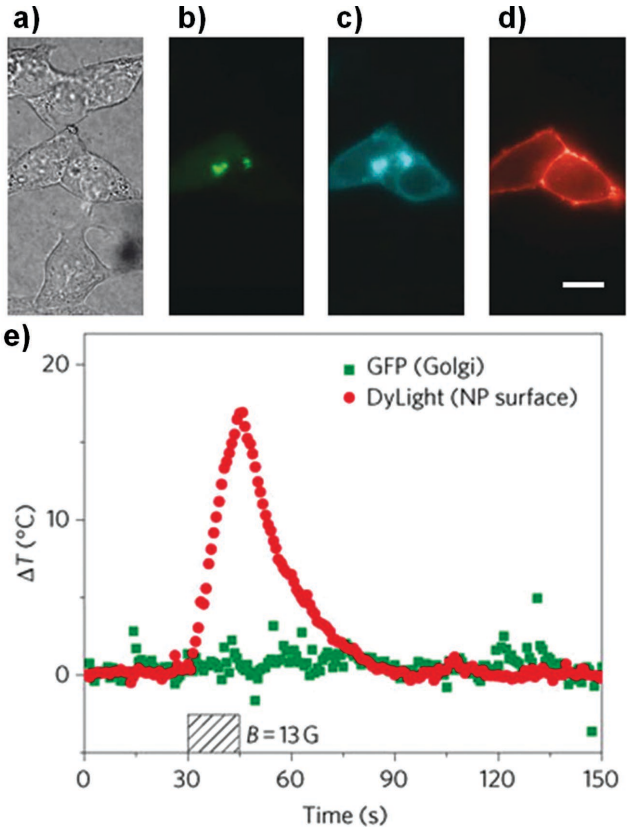

Figure 1. Temperature sensing of the HEK293 cells by using DyLight549-coated $MnFe_2O_4$ nanoparticles. a) Differential interference contrast (DIC) images. b) Green fluorescence image of Golgi apparatus labeled with GFP. c) Cyan fluorescence marking the membrane protein. d) red fluorescence image of the DyLight549-coated nanoparticles. Scale bar, 20 mm. e) the local temperature increased at the plasma membrane (red, measured by the change in DyLight549 fluorescence intensity), after the application of the RF magnetic field (as indicated by the hatched box). Reproduced with permission.[36] Copyright 2010, Nature Publishing Group.

with increasing temperature because of the competition between the luminescence and nonradiative energy transfer from the Eu(III) ion to the ligand (**Figure 3**a and b).[4,41,82] Because of its hydrophobic nature, Eu-TTA was used to integrate into CHO cell membranes for imaging intracellular heat waves after the activation of the m1-muscarinic receptor by acetylcholine (ACH).[41] Fast application of ACh onto the cells can generate a biphasic intracellular heat wave which can be blocked by atropine (Figure 3c). Meanwhile, a typical calcium wave can be activated by ACh that has a much longer latency and duration than the typical heat wave. This thermal imaging technique provided the first example of receptor-activated metabolic heat generation in single living cells and new insights into cellular activities. However, the fluorescence intensity was also sensitive to the pH value of solution.[42,83] Suzuki et al. used a glass micropipette filled with Eu-TTA dissolved in dimethylsulfoxide (DMSO), and measured the cellular temperature changes of a single HeLa (human epithelial carcinoma) cell.[42] By this thermometer, the heat production caused by the ionomycin-induced calcium ion influx from extracellular fluid was observed.[42,84] And the temperature increase was suppressed when Ca^{2+}-ATPases were blocked by thapsigargin. Since the micropipette method afforded a low spatial resolution, they designed fluorescent nanoparticles (**Figure 4**a), in which Eu-TTA was embedded in a poly(methylmethacrylate) (PMMA) network.[43] The fluorescence intensity was not affected with the condition of pH (4–10) and ionic strength (0–500 mM). With a hydrodynamic diameter of 211 nm, these nanothermometers easily entered living HeLa cell by endocytosis, enclosed in acidic organelles (endosome/lysosome) (Figure 4d), and then transported along microtubules in a temperature-dependent manner. The spatial and temperature resolutions of these "walking nanothermometers" are 5.3 nm and 0.3 °C, respectively.

Ruthenium (II) tris(bipydidyl) ion ($Ru(bpy)_3^{2+}$) is another metal complex that can be used as a luminescent temperature indicator. The emission of $Ru(bpy)_3^{2+}$ arises from the electronic transition from a triplet metal-to-ligand charge transfer (^{3}MLCT) state, which could be thermally deactivated.[44,85] Yang et al. prepared $Ru(bpy)_3^{2+}$-doped silica nanoparticles for intracellular temperature sensing.[44] Luminescence of the resulting nanosensors is immune to the quenching by oxygen thanks to the protection of outer silica shell, and is rather sensitive to temperature in the physiological range (25–45 °C) with a sensitivity of –1.26%/°C. After further modification of poly L-lysine, the nanosensors were easily introduced into living HepG2 (human hepatocellular carcinoma) cells along with gold nanorods. A local temperature rise in living cells was monitored, which was caused by gold nanorods after the laser irradiation at 808 nm.

2.3. Inorganic Materials

2.3.1. Quantum Dots

Quantum dots (QDs) are attractive candidates for intracellular thermometers, mainly owing to their small size, adjustable fluorescence, remarkable photostability, and commercial availability. They present temperature-dependent photoluminescence (intensity changes or emission wavelength shifts), and acceptable biocompatibility after suitable surface modification.[86,87] Furthermore, QDs as temperature sensors are resistant to pH (5–7) and other environmental variations that are very important for the design and development of the cellular thermometry.[88] A lot of progress has been achieved by Yang et al. for using QDs as intracellular thermometers.[47,89,90] In an earlier report, they studied the individual CdSe QDs (7–12 nm in diameter) and observed that the emission spectra of a single QD exhibited a red-shift to a longer wavelength as the temperature increased (**Figure 5**a).[89] The temperature sensitivity is approximately 0.1 nm $°C^{-1}$ over a range of 24.4 to 43.6 °C, consistent with the result of previous bulk measurements (0.093 nm $°C^{-1}$). However, their observation indicated that it is not advisable to measure absolute temperatures based on the results of a single QD. The average results of QDs group are more precise and reproducible. After that they performed several studies on NIH3T3 cells using QD655 (CdSe/ZnS core/shell QDs), which has a 0.057 nm $°C^{-1}$

DOI: 10.1002/smll.201600665

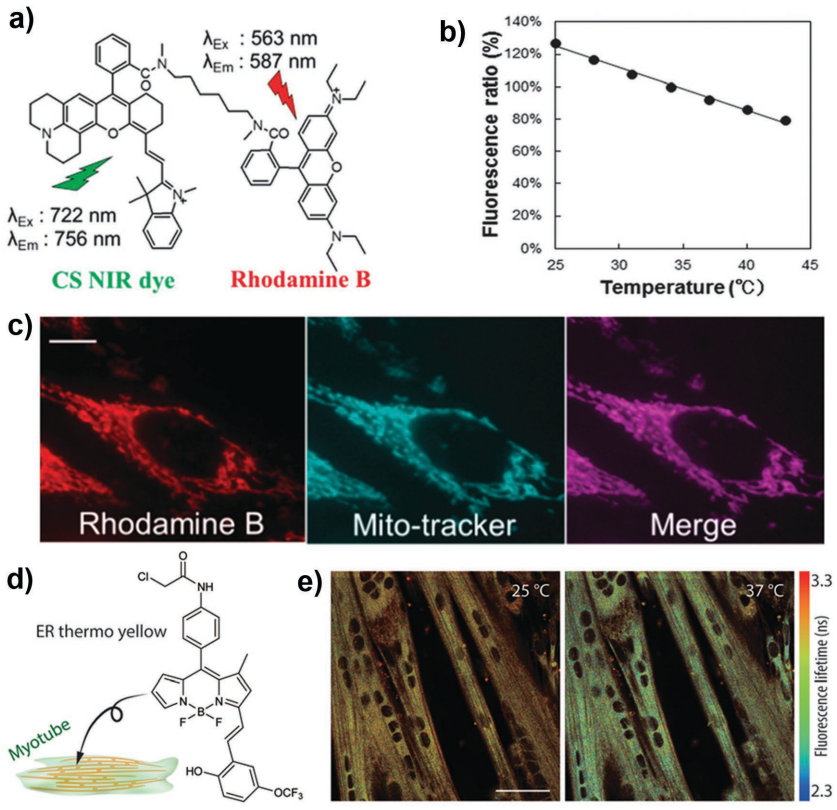

Figure 2. Organelle thermosensing using small-molecule dyes targeting mitochondria (a–c) and endoplasmic reticulum (d). a) Chemical structure of Mito-RTP: thermosensitive rhodamine B and thermoinsensitive CS NIR dye were conjugated to each end of the linker. b) The fluorescence intensity ratio (rhodamine B/CS NIR dye) was determined at various temperatures (normalized at 34 °C). c) Localization of Mito-RTP in living HeLa cells. Scale bar, 5 μm. Reproduced with permission.[40] Copyright 2015, the Royal Society of Chemistry. d) Chemical structure of ER thermo yellow and fluorescence lifetime images of living C2C12 myotubes loaded with ER thermo yellow at 25 °C and 37 °C. Scale bar, 50 μm. Reproduced with permission.[38] Copyright 2016, the Royal Society of Chemistry.

resolution in the cellular environment.[47,90] With the help of streptavidin-QD655, a temperature increase of 1.5 °C was observed in NIH3T3 cells after the infusion of calcium ions.[90] The photoluminescence spectral shifts from endocytosed QDs could be allowed for mapping intracellular heat generation under Ca^{2+} stress and cold shock (Figure 5b–d). The inhomogeneous intracellular temperatures rise can be directly observed.

More remarkably, the thermal sensitivity and stability of QDs can be significantly enhanced by surface modification and optical equipment.[45,49,91] The linkage of thiolated cyclodextrin with aqueous CdTe QDs dramatically enhanced the sensitivity to 0.28 nm $°C^{-1}$, 2.4-fold higher than those of monothiol-ligand-decorated QDs, and suppressed the size alteration of QDs both in the presence of N_2H_4 and under elevated temperature.[91] Polymer-encapsulated QDs, CdSeS/ZnS QDs in the matrix material of poly(methyl methacrylate-co-methacrylic acid) (PMMA-co-MAA), showed non-sensitivity to pH and ionic strength, as well as ultra-high reversibility.[49] Besides, two-photon fluorescence microscopy was used to measure the temperature evolution of HeLa cells applying CdSe QDs as nanothermometers.[45] The fluorescence intensity excited by two-photon provided higher temperature sensitivity than that obtained under one-photon excitation. The use of the two-photon fluorescence microscope excited with near-infrared (NIR) light not only provided much better spatial resolution (below 100 nm), but also reduced specimen photodamage and enhanced penetration depth.[92,93]

2.3.2. Upconverting Nanoparticles

Apart from QDs, lanthanide-doped fluorescent nanoparticles have been developed for intracellular thermosensing. These nanoparticle can convert NIR excitation light to high-energy light (ultraviolet, visible or NIR light) via multiphoton upconversion process.[94] Compared with fluorophores or QDs, these upconverting nanoparticles can be stimulated by low power and inexpensive NIR lasers, which is capable of deep tissue penetration. The variation of particle size also has no effect on the absorption/emission maxima.[50] Vetrone et al. devised a nanothermometer based on the temperature-sensitive fluorescence of $NaYF_4$:Er^{3+},Yb^{3+} NPs, where the intensity ratio of the green florescence bands of the Er^{3+} dopant ions ($^2H_{11/2}\rightarrow{}^4I_{15/2}$ and $^4S_{3/2}\rightarrow{}^4I_{15/2}$) changes with temperature.[50] The nanothermometers are capable of accurately determining the temperature of solutions as well as biological systems such as HeLa cancer cells.

2.3.3. Metal Nanoclusters

Metal nanoclusters has been considered as fluorescent nanothermometers, due to ultrasmall size (< 2 nm in diameter), colloidal stability, good biocompatibility, and facile synthesis.[53,55,95] Shang et al. reported that the lifetime of gold nanoclusters (AuNCs) dramatically decreased with increasing temperature in the physiological range (**Figure 6**a).[53] They also found that the temperature-induced lifetime reduction is dependent on the environment. The lifetime versus temperature behavior in living cells is different from that in buffer solution. The calibration of these AuNCs should be carefully implemented in living cells. Using FLIM, intracellular temperatures of HeLa cells were mapped after the internalization of AuNCs by endocytosis (Figure 6b). Similarly, copper nanoclusters (CuNCs) have also been employed as a fluorescent probe for temperature sensing and cellular imaging.[55,96] CuNCs prepared by Wang et al. were stabilized by glutathione (GSH) and possessed quantum yield up to 5.0%, higher than that of the CuNCs prepared in the previous works.[55] GSH was used as both the reducing agent and the protective layer preventing the aggregation of

DOI: 10.1002/smll.201600665

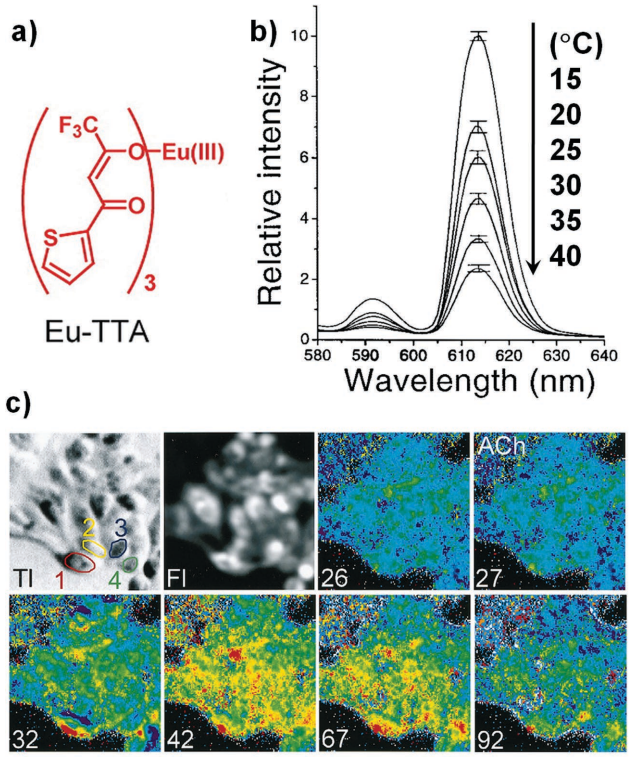

Figure 3. Thermal imaging of living CHO cells using EuTTA in response to a brief application of ACh. a) Chemical structure of Eu-TTA. b) Dependence of Eu-TTA emission intensity on temperature while integrated in liposomal membranes (pH 7.4). c) Transmitted light (Tl), luminescence (Fl) and consecutive pseudo-color images taken before and after the ACh treatment. The numbers on the images are the frame numbers (frame interval ≈1 s). Reproduced with permission.[41] Copyright 1998, Elsevier.

formed nanoclusters. The emission intensity of copper nanoclusters decreased when the temperature rose from 15 to 80 °C. The GSH-CuNCs exhibited good biocompatibility and easy penetration into MC3T3-E1 cells (even cellular nucleus) and monitored intercellular temperature by the help of laser-scanning confocal microscopy.

2.3.4. Nanodiamonds

Recently, nanodiamonds (NDs) have been reported as thermal sensors by some researchers at the same year.[54,97–99] Temperature-sensing ability of NDs comes from the nitrogen-vacancy (NV) center, which is a molecular impurity in the diamond crystal comprised of a substitutional nitrogen impurity adjacent to a carbon vacancy.[97] The electronic ground state of each NV center is split into two energy sublevels under the manipulation of microwave pulse. The precise value of the transition frequency between the levels is highly dependent on temperature. Thus, the principle of NDs is based on accurate measurement of the transition frequency changes.[54,100,101] Kucsko et al. introduced both NDs and gold nanoparticles (light-induced nanoheaters) into human embryonic fibroblast WS1 cell using nanowire-assisted delivery, and temperature variation was precisely measured (**Figure 7**).[54] This method probably provides the highest temperature resolution (0.044 °C) so far. Nevertheless the introduction of NDs into cells using nanowires is an invasive and complicated operation, which greatly restricts the application.

2.4. Thermoresponsive Synthetic Polymers

Polymeric intracellular thermometer composed by thermoresponsive polymers and fluorophores was first demonstrated by Gota et al. based on Poly(N-isopropylacrylamide) (PNIPAM).[17] In this work, the fluorescent nanogel thermometer (FNT) consisted of PNIPAM and a water-sensitive fluorophore (DBD-AA), as displayed in **Figure 8**A. At a low temperature, the polymer is in a fully swollen state and will absorb water into its inner part, leading to the quenching of DBD-AA by neighboring water molecules. When the temperature increases, the polymer shrinks to form a colloidal nanoparticle, and DBD-AA changes to be fluorescent after the release of water molecules. It is well designed to be very stable and pH insensitive, by avoiding interactions with cellular components and removing undesirable fluorescence quenching. A practical use of the FNT was confirmed by measuring intracellular temperature variations of COS7 cells induced by external chemical stimuli. They were internalized into COS7 cells by the means of microinjection, and provided a temperature resolution of 0.29–0.50 °C over the range of 27–33 °C. They found that temperature variation was different among the cells after the treatment of camptothecin. Similarly, Qiao et al. reported an intracellular thermometer based on a block copolymer, consisting of fluorescent and temperature responsive units.[56] The fluorescence intensity decreased with the temperature increase from 24 to 44 °C due to heat-induced block copolymer aggregates. It was successfully applied in the intracellular temperature sensing of MDCK (Madin–Darby canine kidney) cells.

However, the above described nanogel thermometer could not provide a intracellular temperature distribution map, since the relatively large size (≥ 62 nm in hydrodynamic diameter) and low hydrophilicity of the nanogel hindered the spreading throughout the cell. In 2012, the first method for mapping the temperature distribution inside living cells has been demonstrated by Okabe et al., which was improved on this basic.[57] This novel fluorescent polymeric thermometer (FPT) consisted of the same units, but with a reduced size (8.9 nm in hydrodynamic diameter) and an improved hydrophilic behavior, permitting the diffusion throughout a living cell. The three units of FPT can be observed in **Figure 9**A: a thermosensitive unit, a hydrophilic unit, and a fluorescent unit. The fluorescence lifetime of FPT is temperature-dependent. With the help of FLIM, the spatial resolution of FPT reached a diffraction-limited level (200 nm). At a low temperature, the fluorescence is quenched by water molecules in the swelling structure, leading the reducing of the fluorescence lifetime. The lifetime increases with the temperature due to the shrinking structure (Figure 9B), providing a temperature resolution of 0.18–0.58 °C. This method successfully performed temperature mapping in living COS7 cells at the organelle level (Figure 9c). It was found that the nucleus

DOI: 10.1002/smll.201600665

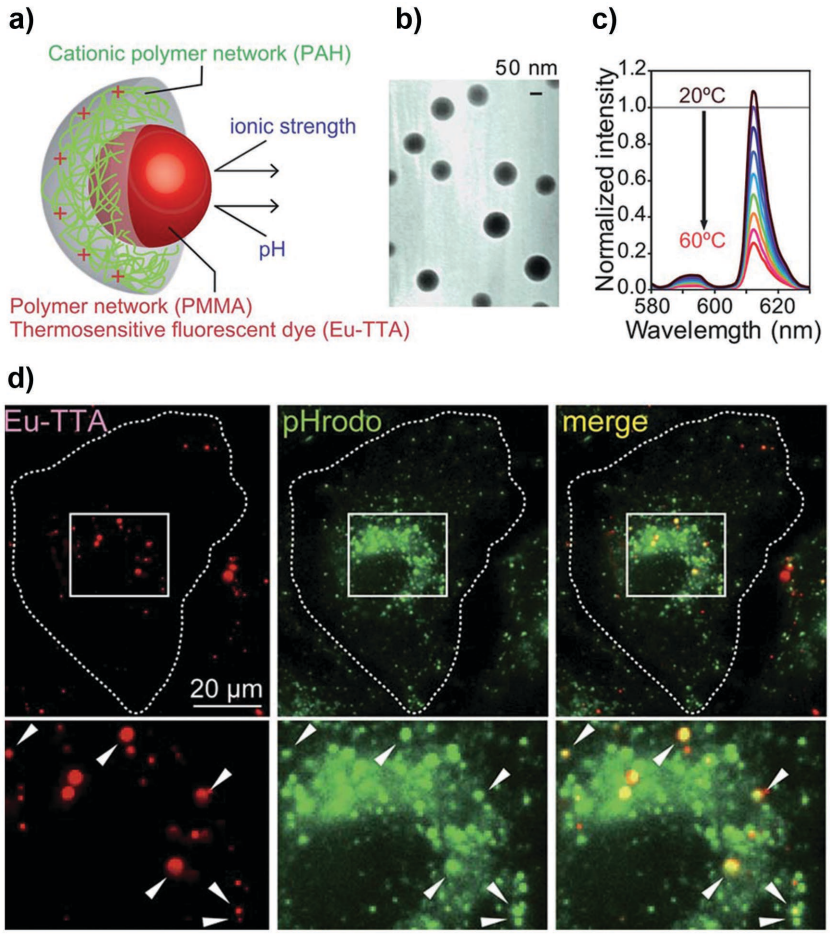

Figure 4. Temperature measurement of living HeLa cells using the fluorescent nanothermometer composed of a polymer network (PMMA) and thermosensitive fluorescent dye (Eu-TTA). a) Schematic diagram of this nanothermometer. b) The core of nanothermometers observed by transmission electron microscopy. c) Fluorescence spectrum of the nanothermometers dispersed in PBS (pH 7.4) at various temperatures. d) Fluorescence images of nanothermometers (Eu-TTA), endosomes/lysosomes labeled with pHrodo-dextran, and merged. Reproduced with permission.[43] Copyright 2012, the Royal Society of Chemistry.

and centrosome showed a significantly higher temperature than the cytoplasm, with an average difference of 0.96 °C (Figure 9d). The local heat production from mitochondria was also observed. However, in this method, the microinjection technique was still required to introduce fluorescent thermometers into mammalian cells. It was not user-friendly and inefficient, and could not be used in small cells or cells with a cell wall, such as yeast. An improved cationic FPT (NN-AP2.5) by the same group effectively solved this problem.[58,59] This cationic fluorescent thermometer contains three units (**Figure 10**a): a thermoresponsive unit (NNPAM: N-n-propylacrylamide), a fluorescent unit (DBD-AA), and a cationic unit (APTMA: (3-acrylamidopropyl)trimethylammonium) that can support the uptake of proteins and genes from the extracellular matrix into a living cell. After easy incubation with yeast cells *Saccharomyces cerevisiae* strain SYT001 at 25 °C for 10 min, NN-AP2.5 rapidly entered into cells and retained stably in the cytoplasm (Figure 10c). Spontaneous entry of the cationic thermometer was also observed in MOLT-4 (human acute lymphoblastic leukemia) and HEK293T (human embryonic kidney) cells. It demonstrated that NN-AP2.5 could be extended to the measurement of intracellular temperature of mammalian cells.

2.5. Biomolecules

Although very rare, there are also some reports tried to develop biomolecule-based thermometers on proteins or DNA, presenting better spatial resolution owing to small molecular size.[12,61–63] The green fluorescent protein (GFP) is widely used as fluorescent markers for cell imaging. In contrast to ectogenous chemical probes, GFP can precisely target to defined organelles and

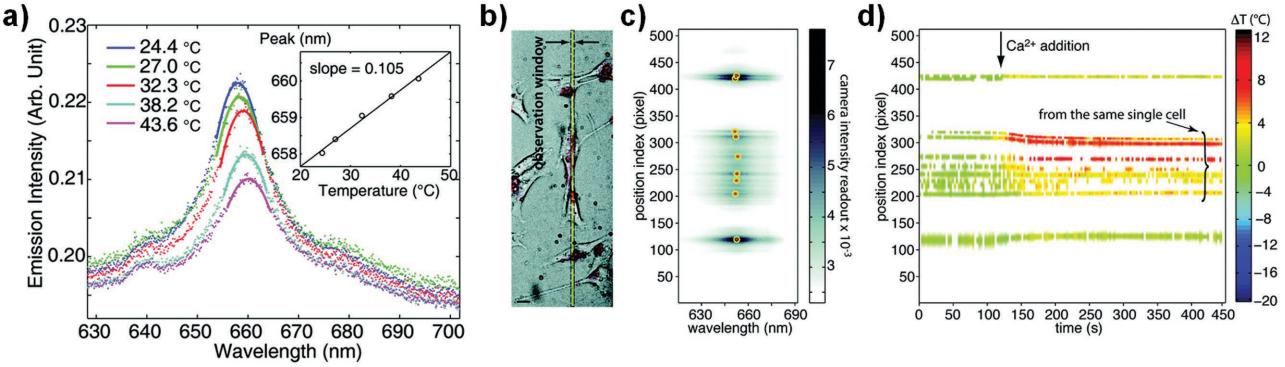

Figure 5. Intracellular thermosensing of living NIH3T3 cells using streptavidin-coated QDs. a) Temperature-dependent spectral shifts of a single QD from 24.4 to 43.6°C. Reproduced with permission.[89] Copyright 2007, American Chemical Society. b) A bright-field micrograph of cells overlaid with QDs emission image. c) Representative snapshot of the raw position-spectrum maps for the sample shown in (b). d) Location-dependent intracellular temperature progression as a function of time of the same cell shown in c). Reproduced with permission.[47] Copyright 2011, American Chemical Society.

DOI: 10.1002/smll.201600665

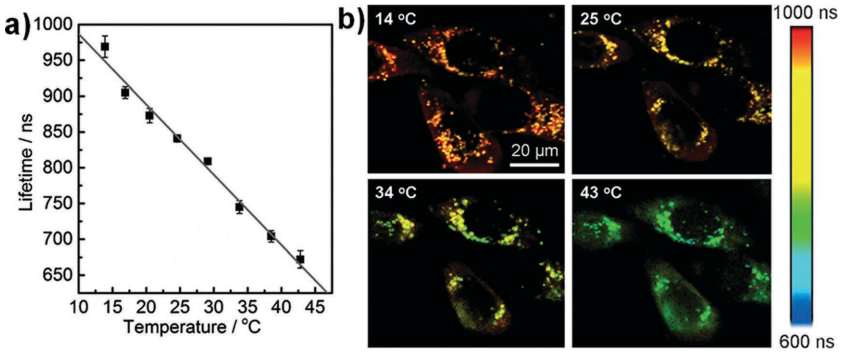

Figure 6. Intracellular thermometry of living HeLa cells using fluorescent gold nanoclusters (AuNCs). a) Fluorescence lifetime of AuNCs in living cells versus temperature. b) Typical fluorescence lifetime images of HeLa cells with internalized AuNCs at for different temperatures. Reproduced with permission.[53] Copyright 2013, Wiley-VCH.

will not disrupt cellular activities if appropriately designed. Donner et al. developed GFP-based thermometers for monitoring intracellular thermogenesis.[61] The fluorescence polarization anisotropy (FPA) of GFP is strongly temperature dependent, decreases linearly with temperature in the physiological range (20–60 °C, **Figure 11**b). The FPA of the GFP is defined as a ratio of the intensities of the fluorescence polarized parallel and perpendicular to the incident polarization, and not sensitive to absolute intensity changes caused by uncontrollable factors, making the results more reliable. It was also interesting to find that the calibration curve (FPA vs temperature relationship) obtained inside the cells was significantly different to that in buffer solution due to the viscosity difference. This observation indicated that the calibration should be performed for each cell line to be studied. The method is tested on GFP-transfected HeLa and U-87 MG (human glioblastoma-astrocytoma) cancer cell lines. They monitored the heat delivery by photothermal heating of gold nanorods surrounding the cells (Figure 11c–e).[61] In addition to this, they extended this method to a living organism and present the first in vivo intracellular temperature imaging of *Caenorhabditis elegans (C. elegans)*.[12]

The thermal sensitivity of GFP-based thermometers (tsGFPs) was further improved by Kiyonaka et al. and enabled the visualization of thermogenesis in discrete organelles in living cells.[62] The thermosensitive coiled-coil protein TlpA, an autoregulatory repressor protein in *Salmonella* that senses temperature changes and controls transcription repression in a temperature-dependent manner, was used to build tsGFPs. A GFP is inserted between tandemly repeated coiled-coil regions of TlpA. The thermosensing capability is derived from a rapid and reversible structural transition of TlpA from

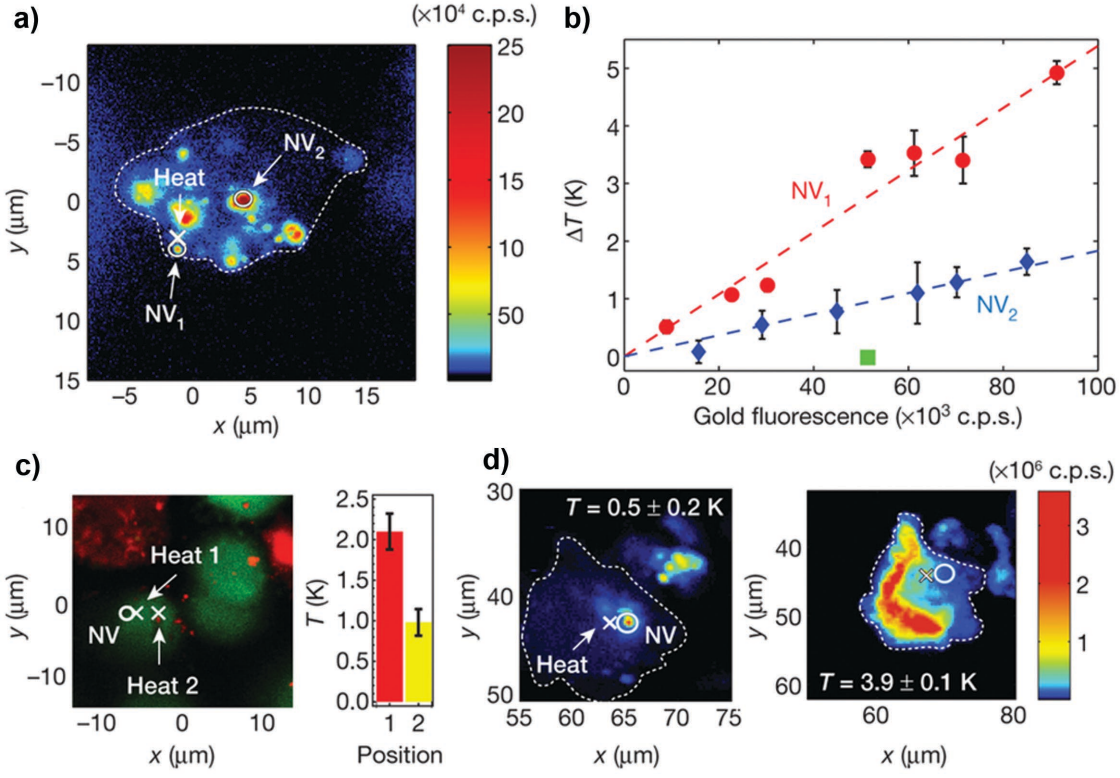

Figure 7. Intracellular temperature measurement using nanodiamonds (nitrogen-vacancy centers in diamond nanocrystals). a) Confocal image of nanodiamonds in a single WS1 cell. The cross marks the position of the gold nanoparticle used for heating, and circles represent the location of the nanodiamonds (NV_1 and NV_2) used for thermometry. b) Temperature at the position of NV_1 and NV_2 changes with the incident laser power applied to the gold nanoparticle. c) Temperature of o single nanodiamond (circle) with local heat applied at two different locations (crosses). d) Confocal fluorescence images indicate the cell death under laser illumination. Reproduced with permission.[54] Copyright 2013, Nature Publishing Group.

DOI: 10.1002/smll.201600665

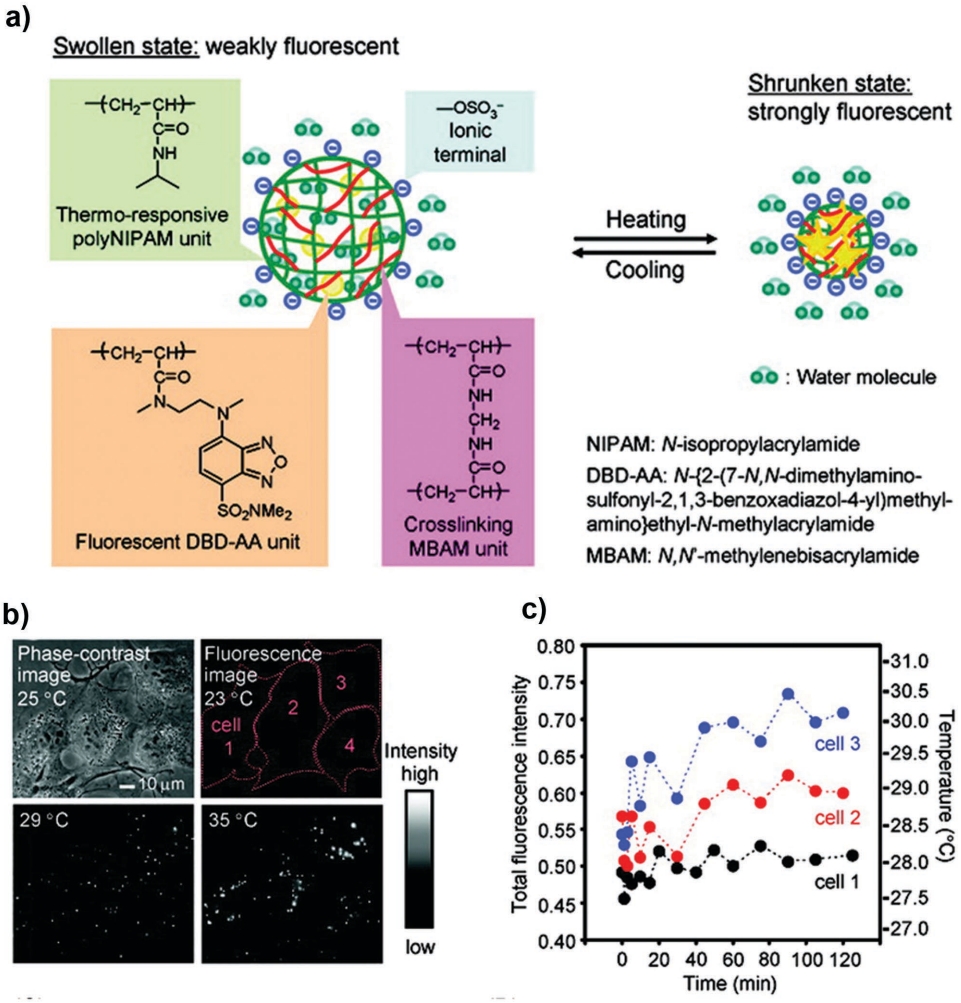

Figure 8. Intracellular thermosensing of living COS7 cells using fluorescent nanogel thermometer (FNT). a) Schematic diagram and chemical structures of the FNT. b) Phase-contrast and fluorescence images of living COS7 cells containing FNT. c) Fluorescence intensity changes of FNT in three living COS7 cells (left axis) and the corresponding temperature (right axis) after the additions of camptothecin. Reproduced with permission.[17] Copyright 2009, American Chemical Society.

a parallel coiled-coil dimer to two unfolded monomers at around 37 °C, which will be transmitted to GFP, thus eliciting a measurable temperature-dependent fluorescence change (**Figure 12**a). Temperature rise from 20 to 50 °C increases the intensity of the 480 nm peak and decreases that of the 400 nm peak (Figure 12b). Figure 12c shows the temperature dependence of ex400/ex480 intensity ration as a function of temperature. The sensitivity lies in the linear region (38–46 °C) is 3.5 times higher than that of GFP. Besides, the temperature-sensing range of tsGFPs can be controlled by selecting the suitable coiled-coil region from TlpA. They monitored the temperature changes in ER and mitochondria of living HeLa cells by fusing specific organelle-targeting sequences to tsGFPs.[62] As shown in Figure 12d–e, the heterogeneous thermogenesis of mitochondria was clearly observed after the treatment of carbonyl cyanide 3-chlorophenylhydrazone (CCCP). The thermogenesis processes in brown adipocytes and skeletal muscle myotubes were also visualized.

Other than GFP, molecule beacons are functional engineered nucleic acid molecules that can selectively interact with a target DNA or RNA sequence, and has been widely applied in many bio-sensing areas. Ke et al. reported an intracellular thermometer based on L-DNA (isomer of natural D-DNA) molecular beacons (L-MBs).[63] A molecular beacon is a hairpin-structured DNA molecule dually labeled by a fluorophore and a quencher at two opposite ends (**Figure 13**a–b). The distance between the fluorophore and quencher changes with temperature. At a low temperature, the beacon has low fluorescence due to the closed hairpin, but becomes highly fluorescent with the temperature increasing. L-MBs were introduced into living HeLa cells via liposome transfection and distributed in the nucleus, and became highly fluorescent when the temperature increased from 20 °C to 37 °C (Figure 13c–d). In this issue, the utilization of non-natural L-DNA is crucial for the stability in a complex cellular environment. Since D-DNA-based molecular beacons (D-MBs) were believed to be completely digested by intracellular nucleus, they were unable to respond to temperature changes (Figure 13e). Then Ebrahimi et al. designed a multiplex MB probe using gold nanoparticles as quenchers, on which many MBs of more than one type were immobilized.[102] In this design, 13 nm gold nanoparticles were labeled with three types of MBs with

DOI: 10.1002/smll.201600665

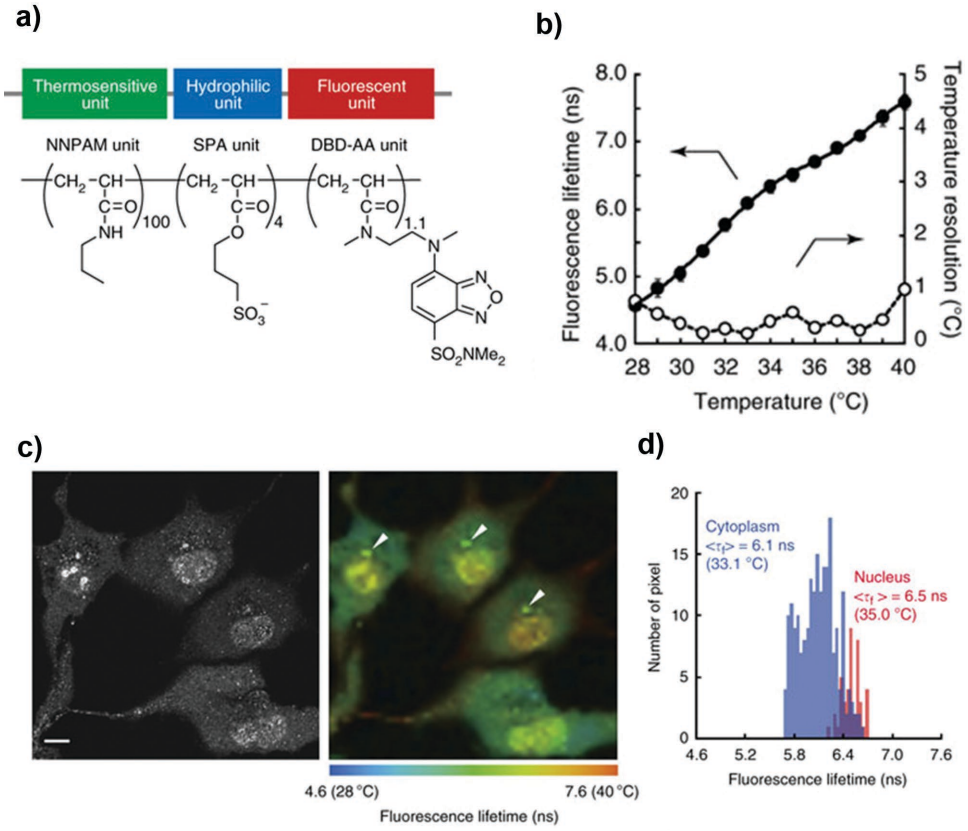

Figure 9. Intracellular temperature mapping of living COS7 cells with fluorescent polymeric thermometer (FPT). a) Chemical structure of FPT. b) Calibration curve (closed, left axis) and temperature resolution (open, right axis) of FPT. c) Temperature mapping in living COS7 cells: Confocal fluorescence image (left) and fluorescence lifetime image (right) of FPT. d) Histograms of the fluorescence lifetime in the nucleus and in the cytoplasm in a representative cell showing a higher temperature in the nucleus. Reproduced with permission.[57] Copyright 2012, Nature Publishing Group.

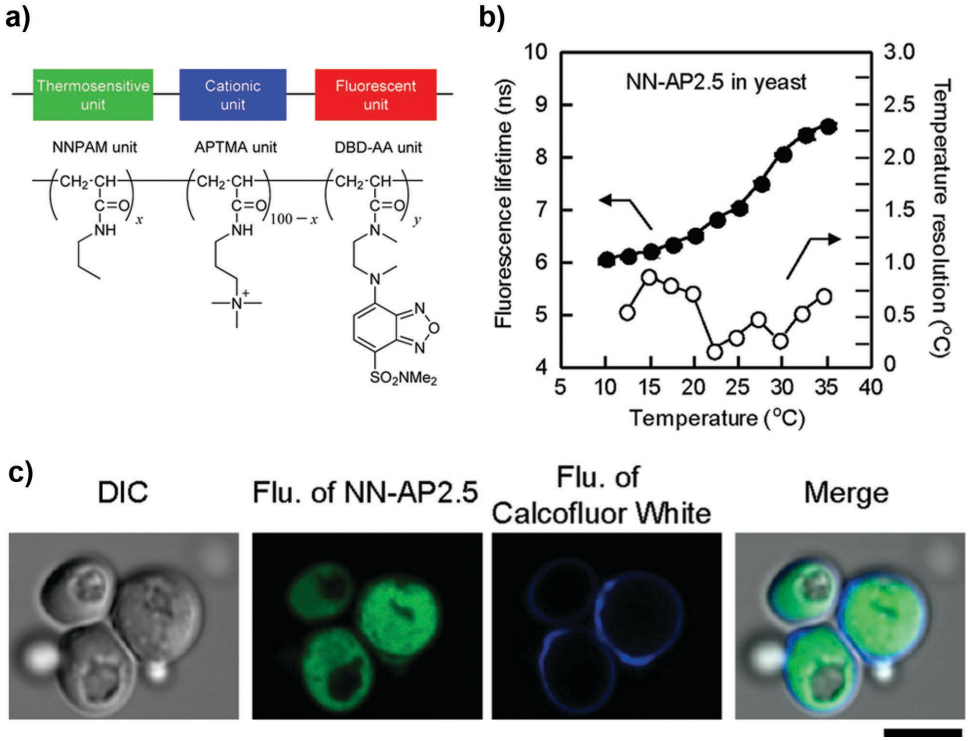

Figure 10. Intracellular temperature measurement of living yeast cells using cationic fluorescent polymeric thermometer NN-AP2.5. a) Chemical structure of NN-AP2.5. b) Fluorescence lifetime response and temperature resolution of NN-AP2.5 in yeast cells. c) Intracellular localization of NN-AP2.5 in yeast cells. DIC and confocal fluorescence images of NN-AP2.5 and cell wall. Reproduced with permission.[58] Copyright 2013, American Chemical Society.

DOI: 10.1002/smll.201600665

www.MaterialsViews.com

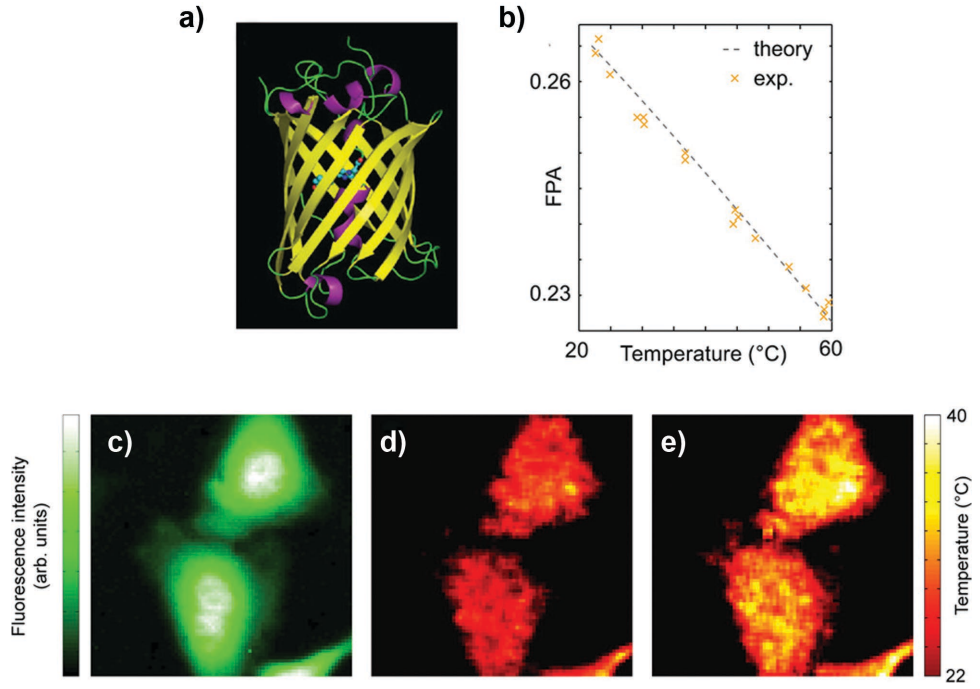

Figure 11. Intracellular temperature mapping of Hela cells using green fluorescent protein (GFP). a) Structure of GFP. b) Calibration curve that relates between FPA of GFP and temperature in PBS. c-e) Temperature measurements in HeLa cells while heating via the photothermal approach: c) fluorescence intensity of GFP transfected HeLa cells, d) temperature map while not heating, e) temperature map while heating the nanorods with a focused infrared laser. Reproduced with permission.[61] Copyright 2012, American Chemical Society.

different thermostabilities, providing a wide temperature sensing range. The temperature resolution of the nanoprobes is less than 0.5 °C over a range of 15–60 °C.

3. Contact Thermometry

In addition to contactless (luminescent) thermometers, a number of contact thermometric techniques have been developed for cell thermal sensing, primarily electrical and mechanical thermometers. The developments of nanolithography and microelectromechanical systems (MEMS) make it possible for fabricating thermal probes with sub-micrometer size and miniaturize the conventional thermometers with geometrical size at submicroscale.

The thermocouple is the most commonly used macro thermometer, which employs the Seebeck effect of thermal

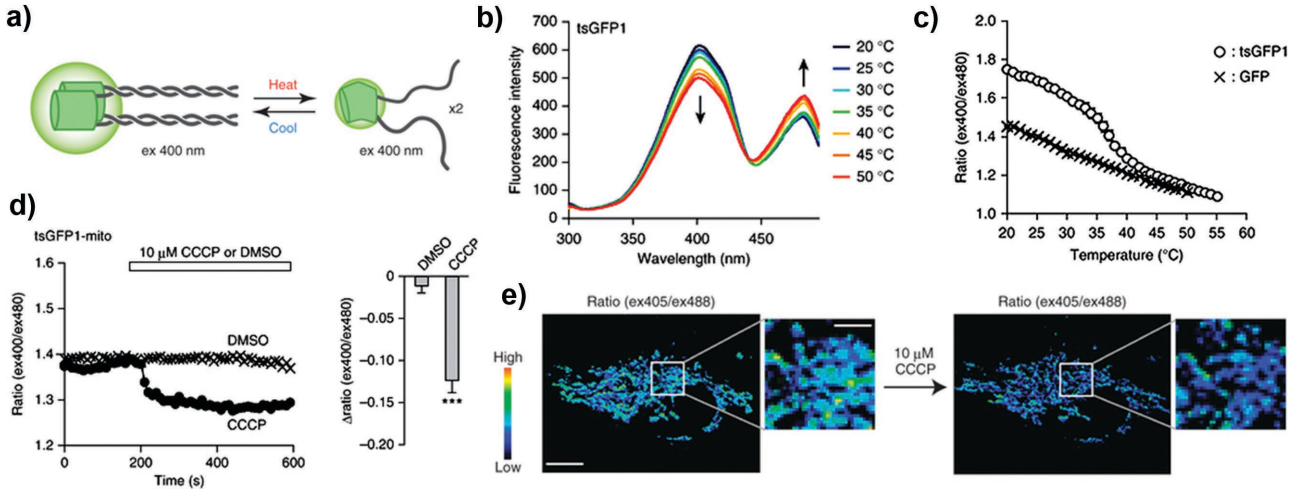

Figure 12. Monitoring Subcellular thermogenesis using a GFP-based thermosensor tsGFP1. a) Schematic diagram of tsGFP1, which is composed of GFP and coiled-coil regions of TlpA. The tandem formation of the coiled-coil structure is associated with thermal changes resulting fluorescence change of tsGFP1. b) Fluorescence excitation spectra of tsGFP1 at various temperatures. c) Temperature-dependent changes in the ex400/ex480 ratio of tsGFP1 and GFP. d) Fluorescent responses in tsGFP1-mito-expressing HeLa cells at 37 °C after the treatment of CCCP and DMSO, respectively. e) Pseudocolor confocal images of fluorescence intensity ratio in tsGFP1-mito-expressing HeLa cells after the treatment of CCCP. Reproduced with permission.[62] Copyright 2013, Nature Publishing Group.

DOI: 10.1002/smll.201600665

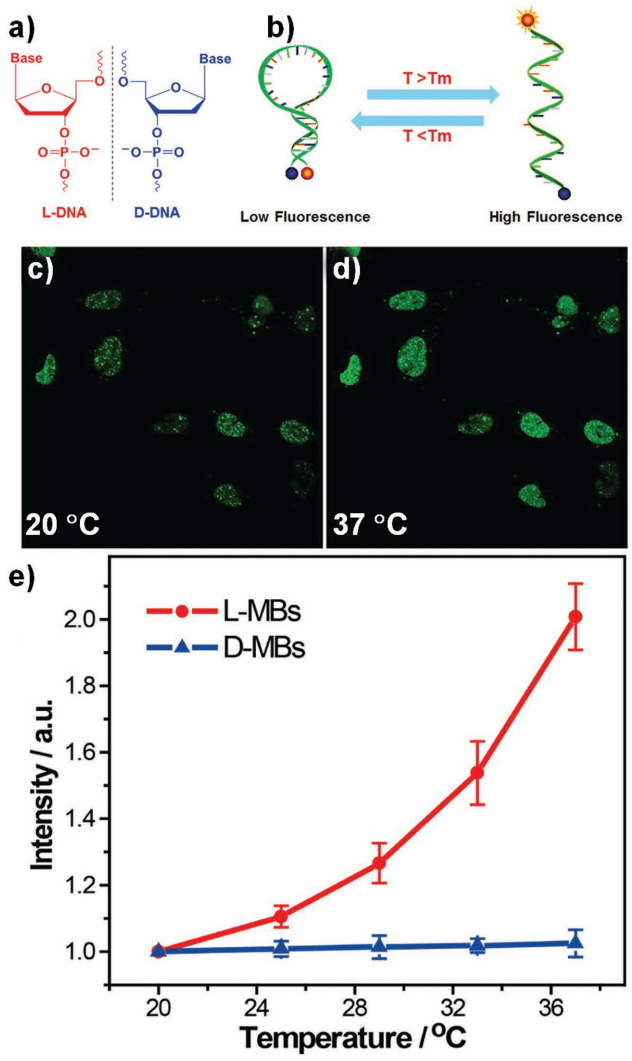

Figure 13. Intracellular temperature sensing of living HeLa cells using L-MB. a) Structure of L-DNA. b) Principle of the L-MB-based intracellular nanothermometer. Confocal microscopy images of HeLa cells transfected with L-MBs at different temperatures: c) 20 °C and d) 37 °C. e) Temperature-fluorescence intensity curve of cells transfected with L-MBs and D-MBs (normalized to the fluorescence intensity at 20 °C). Reproduced with permission.[63] Copyright 2012, American Chemical Society.

electric materials to measure temperature based on the heat transmission at the tip-sample contact point.[64,103] Watanabe et al. first produced micro-thermocouple probes for the measurement of cellular thermal responses.[104] In this technique, a junction of two different metal films (Pt-Au) is formed at the glass micropipette tip with a diameter of 1 μm by using microfabrication methods. After that, Shrestha et al. improved the sensitivity of the micropipette-thermocouple by using inexpensive materials.[105] The sensors were fabricated by filling a glass micropipette with Sn-based alloy and coating another metal thin film (Ni) on the outer surface of the pipette by physical vapor deposition (PVD). This thermometer has a spatial resolution of 4 μm and temperature resolution of 0.01 °C. In order to verify the feasibility, they injected the tip of micropipette-thermocouple into a living cell, which was exposed to a green laser beam (at 532 nm) for 1500 ms. The rising time of temperature was revealed at round 600 ms.[105] After that, our group promoted the thermocouple-based method for detecting intracellular temperature.[64,106] In our scenario, the thermocouple (TC) probe has a sandwich structure consisting of the tungsten (W) tip, an insulating layer made of polyurethane (PU), and a platinum (Pt) film (**Figure 14**a). We found that the sensitivity of the TC probes is dependent on the thickness of the Pt film. After the calibration, the temperature-thermoelectricity curve of the probe with 100 nm Pt film matched perfectly with the standard macro-size TC probe, but was different with the probe with 50 nm Pt film. The TC probe can distinguish temperature differences of less than 0.1 °C. For intracellular temperature measurement of a living cell, micromanipulation system is needed for handling precise insertion of the tip into a single U251 cell. Meanwhile, the thermovoltage is recorded by a digital multimeter. Using this method, a temperature increase in a living U251 cell can be observed after the treatment with camptothecin (a DNA topoisomerase I

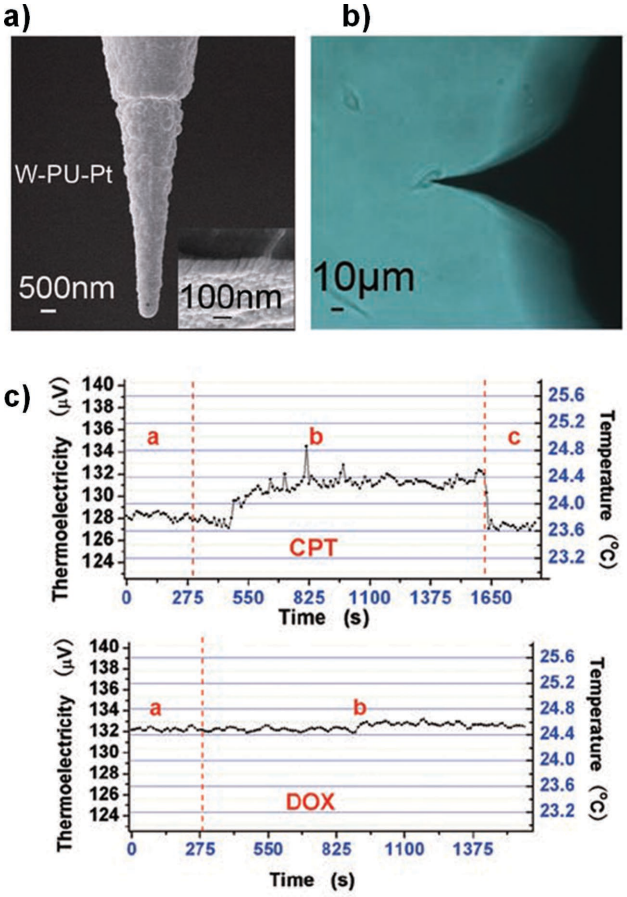

Figure 14. Intracellular temperature determination of U251 cells by a thermocouple method. a) SEM image of the thermocouple: tungsten tip (inner core), polyurethane film (interlayer), and platinum film (outer layer). b) Optical microscopic image of a living U251 cell inserted by the thermocouple probe. c) Intracellular temperature changes of a single U251 cell after the treatment of camptothecin (CPT, upper) and doxorubicin (DOX, lower). a: the thermocouple was inserted into the cell; b: after the addition of CPT or DOX to the culture medium; c: the thermocouple was withdrawn from the cell. Reproduced with permission.[64] Copyright 2011, Nature Publishing Group.

DOI: 10.1002/smll.201600665

inhibitor), but unchanged in the case of doxorubicin (a DNA topoisomerase II inhibitor) (Figure 14b–c).

Another interesting method developed by Inomata et al. can detect the heat released from a single cell.[107] They developed a pico calorimeter containing a heat-detecting Si resonator (resonant thermal sensor). The measurement principle relies on temperature-dependent change in the resonant frequency of the resonator, as heat flows from the sample in water to the resonator in a vacuum. The heat resolution of the fabricated sensor is 5.2 pJ. This device was tested on measuring heat production from a single brown fat cell (BFC) after treatment of norepinephrine, which maintained over approximately 20 min.

4. Composite Structure Thermometry

Up to now, the cellular thermometers above-described mostly give a temperature value from an absolute change of one single temperature-dependent signal, without any additional reference. Especially for the luminescence-based thermometry, it is a valid approximation only when the signal is extracted from the emission spectral position or lifetime decay. However, many of these thermometers are based on thermally induced fluorescence intensity variation. In these cases, the accuracy could be affected by many factors: (1) the environment; (2) the distribution and concentration of the probes; (3) photobleaching; (4) fluctuations in the excitation source; and (5) the efficiency of the detectors, leading to erroneous results and interpretation. Recently, composite thermometers with dual wavelength self-calibration have attracted great attention. Because the ratiometric fluorescent readout is independent of the above factors, it provides a more robust result.

The design of many ratiometric fluorescent thermometers is based on a thermosensitive polymer and the use of two fluorophores.[68,70,75–78,108] Chen et al. synthesized a cross-linked PNIPAM-based fluorescent nanothermometer known as Thermo-3HF (3HF refer to 3-hydroxyflavones).[108] The probe 3-HF displays dual-band emissions associated with normal excited state intramolecular charge and tautomer excited state intramolecular proton transfer. PINPAM switches between swollen and shrunken state at different temperatures, resulting in 3-HFs changes from a bluish to greenish color. The intensity ratio of the two bands provided a sensitive and reversible response to temperature in the range of 33 to 41 °C, providing more sensitive and robust signals. Uchiyama et al. designed a novel cationic fluorescent polymeric thermometer containing both DBThD-AA and BODIPY-AA units as an environment-sensitive fluorophore and as a reference fluorophore, respectively.[76] Except two fluorophore units, it contains two other units: a thermosensitive NNPAM unit and a cationic APTMA unit. The change in the fluorescence ratio at 580 nm to 515 nm (primarily originates from the DBThD-AA and BODIPY-AA units, respectively) was strongly correlated with the temperature from 25 to 45 °C. The temperature resolution was determined to be 0.01–1.0 °C after introduction into the MOLT-4 (human acute lymphoblastic leukemia) and adherent HEK293T (human embryonic kidney) cells. Moreover, fluorescence resonance energy transfer (FRET) is very powerful in detection and sensing, and can be applied in ratiometric fluorescent thermometers. Liu developed a hydrophilic fluorescence temperature probe (PNDP-NR) based on PNIPAM nanogel, and the ratiometric readout was obtained from the FRET between a polarity-sensitive triarylboron compound (DPTB) and Nile Red (NR).[75] Upon heating, the green fluorescence at 470 nm increases, whereas the fluorescence intensity of NR at 625 nm slightly decreases due to the decreasing efficiency of FRET. With this probe, the temperature can be measured directly with a colorimeter or distinguished easily by the naked eye. Based on two-step cascade FRET, thermoresponsive double hydrophilic block copolymers-based fluorescent thermometers were fabricated by Hu et al.[78] CMA (Blue-emitting coumarin monomer), NBDAE (green-emitting NBD monomer), and RhBEA (red-emitting rhodamine B monomer) were copolymerized separately with NIPAM to afford dye-labeled PEG-b-P(NIPAM-co-CMA), PEG-b-P(NIPAM-co-NBDAE), and PEG-b-P(NIPAM-co-RhBEA). In this thermometer, NBD acted as a bridging dye by transferring energy from CMA to RhBEA. Compared with one-step FRET thermometers, the sensitivity was improved significantly and reached as low as ≈0.4 °C in the temperature range of 20–44 °C.

The precision of the thermometers containing two organic dyes decreases with long-term irradiation, which is not good for continuous measurement.[79,109] While inorganic luminescence materials are more photostable.[69,71–74] In the work of Albers et al., the dual-emitting quantum dot/quantum rod-based nanothermometers are conferred by FRET process between CdSe–CdS quantum dot-quantum rods as donors and cyanine dyes as acceptors (**Figure 15**a).[69] Thermometers were immobilized onto the pH-sensitive polymer colloid surface via electrostatic interactions, which served to both improve uptake and release of nanocrystals from endosomal confinement, just as described before.[110,111] The intensity of QD-QR from the region ($I_{630–640}$) undergoes a small change, while Alexa-647 is most temperature responsive at another region ($I_{644–674}$) (Figure 15b). In the temperature range of 20–25 °C, the ratiometric response ($I_{630–640}/I_{664–674}$) exhibited the sensitivity at ≈2.4%/°C (Figure 15c). Takei et al. also developed a ratiometric nanothermometer containing two fluorophores embedded in a polymeric particle: Eu-TTA (the thermosensitive fluorophore) and rhodamine 101 (the thermoinsensitive fluorophore used as a self-reference) (**Figure 16**a–c).[71] They successfully followed the temperature change in a single cell together with the Ca^{2+} burst induced by the Ca^{2+} ionophore ionomycin (Figure 16d–e). The different temperature increase among different spots indicated heterogeneous heat production in the cell.

5. Applications

Much information about the different cellular processes can be reflected in or strongly influenced by the intracellular temperature changes. During recent years, researchers

small 2016,
DOI: 10.1002/smll.201600665

small NANO MICRO

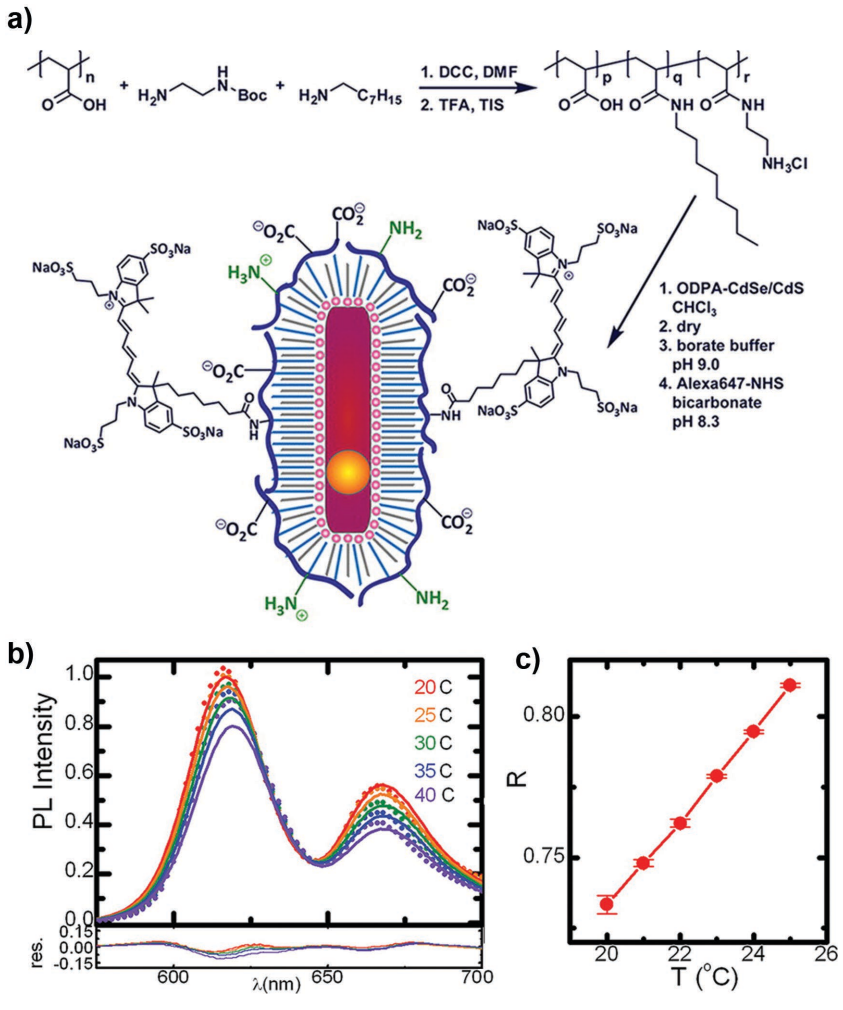

Figure 15. Dual-emitting quantum dot/quantum rod-based nanothermometers (NanoTs). a) Chemical Structure of the nanothermometer. CdSe-CdS quantum dot-quantum rod semiconductor nanocrystal is passivated with an amphiphilic polymer shell, to which is appended with far-red emitting cyanine dyes. b) Calculated (dots) and observed (solid lines) temperature-dependent emission from NanoTs with ≈12 Alexa-647 dyes conjugated to their periphery. c) Ratiometric response of NanoTs for T = 20–25 °C. Reproduced with permission.[69] Copyright 2012, American Chemical Society.

are starting to take advantage of these micro/nanoscale thermometers in cell biology, with high resolution and accuracy in living cells. It has already been found that anti-cancer drug CPT can cause the intracellular temperature variation, which might be due to early responses of apoptosis such as DNA cleavage.[17,64] In cytosol, heat production at the ER in living cells was observed after the treatment of ionomycin, which causes calcium influx from the extracellular medium.[37,47] Carbonyl cyanide 4-(trifluoromethoxy)phenylhydrazone (FCCP) and carbonyl cyanide 3-chlorophenylhydrazone (CCCP) have been demonstrated to lead heat generation in mitochondria, which transports protons across the mitochondrial inner membrane to prevent the coupling of ATP synthesis and oxidative phosphorylation.[40,59,62,71] The temperature difference between the nucleus and the cytoplasm (0.96 °C) was also observed, which may originate from the intense activities of the nucleus (e.g., DNA replication, transcription and RNA processing) and/or from structural separation by the nuclear membrane.[6,57,59]

In addition, one of the most studied applications is the real-time monitoring of hyperthermia for the therapy of cancer.[20,21,46,48,51,52,112,113] First, the accurate measurement of temperature increase around the heaters is crucial for regulating the heat release. Bendix et al. directly measured the temperature surrounding single gold nanoparticles trapped on a lipid bilayer, which had incorporated with fluorescent molecules related to phase transitions of lipid bilayers.[112] The temperature increase ranges from a few degrees to hundreds of degrees Celsius and the heating process can be controlled exactly by a careful choice of gold nanoparticle size and laser power. By using CdSe QDs, Li et al. quantitatively measured the dynamic microscale thermal gradient induced by localized gold nanorods in solutions.[113] Precise temperature mapping with diffraction-limited spatial resolution and the sub-degree temperature resolution was achieved, and the results showed an excellent agreement with theoretical simulations. Besides, Jaque's group has done a lot of work in the temperature monitoring of hyperthermia. They used CdSe QDs to monitor intracellular temperature during plasmonic-mediated hyperthermia of HeLa cancer cells.[46] Both the fluorescence nanothermometers (CdSe QDs) and metallic nanoheaters (gold nanorods) were introduced into cells simultaneously by incubation. Then, a single HeLa cell was illuminated by lasers at the plasmon resonance wavelength (808 nm) of the gold nanorods inside this cell, leading a relevant intracellular heating. The real-time temperature reading was achieved from the spectral analysis of QDs (**Figure 17**). Later, they used neodymium-doped LaF_3 core/shell nanoparticles as subtissue optical probes because of the spectral overlap of the neodymium emission bands with the transparency windows of human tissues.[51] Subtissue penetration length of 2 mm has been demonstrated, which is significantly larger than that achieved by QDs. The precise real-time temperature reading provides a possibility to improve the operation of laser-induced hyperthermia, avoiding the irreversible thermal damage in healthy cells and tissues surrounding, which is crucial in real clinical treatment of patients. In addition to hyperthermia of cancer, they also investigated the laser-induced thermal effects in optically trapped microspheres and single cells by QDs luminescence thermometry.[48] The experimental results revealed that an optimum trapping wavelength exists for biological applications close to 820 nm (**Figure 18**a). In contrast, maximum heating has been found for a trapping wavelength of 980 nm, resulting in cell damage and even cell death due to water

DOI: 10.1002/smll.201600665

www.MaterialsViews.com

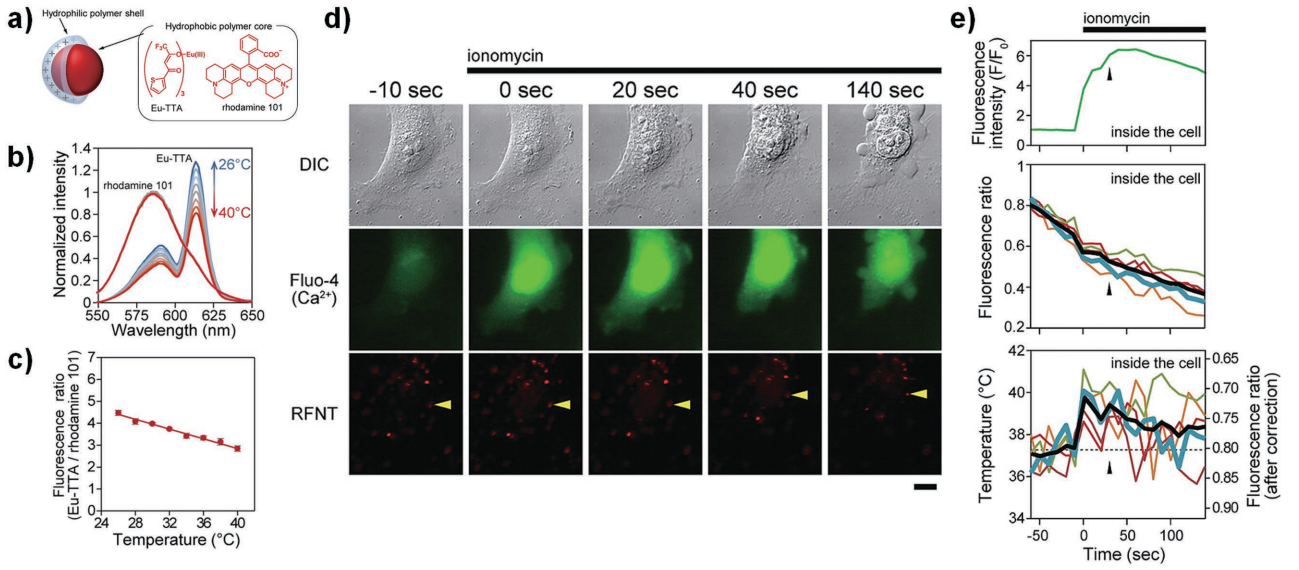

Figure 16. Intracellular thermosensing of living HeLa cells using ratiometric nanothermometer (RNT) composed of Eu-TTA and rhodamine 101. a) Schematic illustration of RNTs. b) Fluorescence spectra of Eu-TTA and rhodamine 101 in the RNT measured from 26 to 40 °C. c) Fluorescence ratio (Eu-TTA/rhodamine 101) at various temperatures. d) Time lapse imaging of DIC (differential interference contrast), Fluo-4 (indicating Ca^{2+} ion) and rhodamine 101 in the RNT after the treatment of the ionomycin–Ca^{2+} complex. e) Time courses of the fluorescence intensity of Fluo-4 (top), the fluorescence ratio of the RNT (Eu-TTA/rhodamine 101, middle), and the temperature (bottom) measured inside the cell. Reproduced with permission.[71] Copyright 2014, American Chemical Society.

absorption at this wavelength (Figure 18b–c), particularly when highly focused laser beams are used.

The above-described dual-particle approaches, which using one nanoparticle for heating and a second nanoparticle for thermometry, have an intrinsic limitation of uncontrolled spatial distribution of nanoheaters and nanothermometers.[72] Thermosensing cannot be achieved at the same position of heaters. Recently, joining nanoheaters and nanothermometers in a single nanoparticle (single-particle approach) has been gradually achieved within last three years.[72,114–116] Freddi et al. bounded rhodamine B to the surface of nanoheaters by electrostatic interaction, monitored accurately the temperature in the close proximity of the nanoheaters (≈20 nm) through its excited state lifetime.[115] In the method of Dong et al., the $NaYF_4$:Yb^{3+},Er^{3+} nanothermometer and the magnetic Fe_3O_4 nanoparticle are encapsulated in the same mesoporous silica nanoparticle, which provides a rigid structure support and isolates the thermometer and heater from the bulk surroundings.[116] Nevertheless, the temperature determination of the heater was not accurate enough, since the thermometer was 8–9 nm from the heater. In another work, Debasu et al. developed a simple and all-in-one nanoplatform, in which $(Gd,Yb,Er)_2O_3$ nanorods (thermometers) were decorated with Au NPs (heaters).[114] The small interparticle distance between thermometer and heater enables to measure the absolute local temperature (not an average temperature) of the sample volume under irradiation, over a wide range (300 to 2000 K). By increasing the amount of Au NPs, the surface temperature of thermometer rises. Whereas the thermometer is overdimensioned relative to the heater, and a high heating power induced by laser radiation is needed. Piñol designed a unique heater/thermometer nanoplatform that overcame the limitations mentioned in the previous studies.[72] In this platform, magnetic NPs (heater) are functionalized with dual-emissive Eu^{3+}/Tb^{3+} lanthanide complexes (thermometer), and then coated with a P4VP-*b*-P(PMEGA-*co*-PEGA) copolymer. The thermometer is located directly on the surface of the heater that

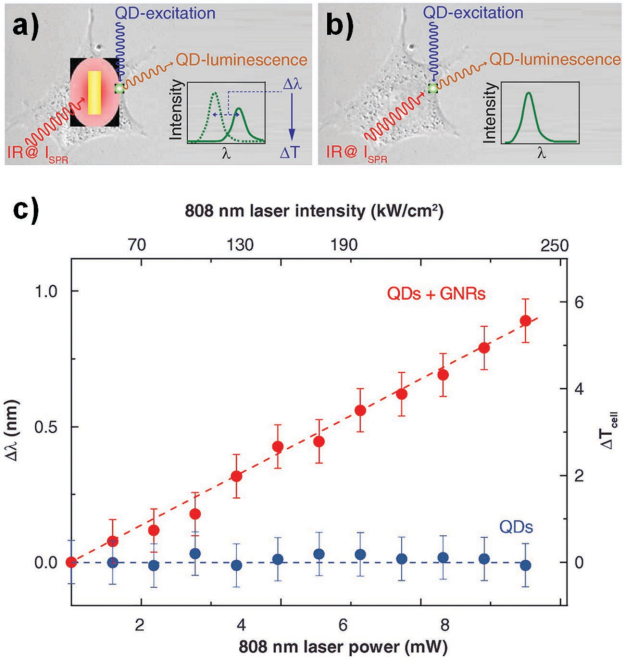

Figure 17. Plasmonic-mediated intracellular hyperthermia monitored by QDs. a) Schematic representation of gold nanorods-assisted intracellular heating and CdSe QDs-mediated thermal reading, both activated by laser. b) Schematic representation of the same effect but in the absence of gold nanorods. c) Intracellular temperature increment of a single HeLa cell as a function of the heating laser power in the presence/absence of gold nanorods. Reproduced with permission.[46] Copyright 2013, Future Medicine Ltd.

small 2016,
DOI: 10.1002/smll.201600665

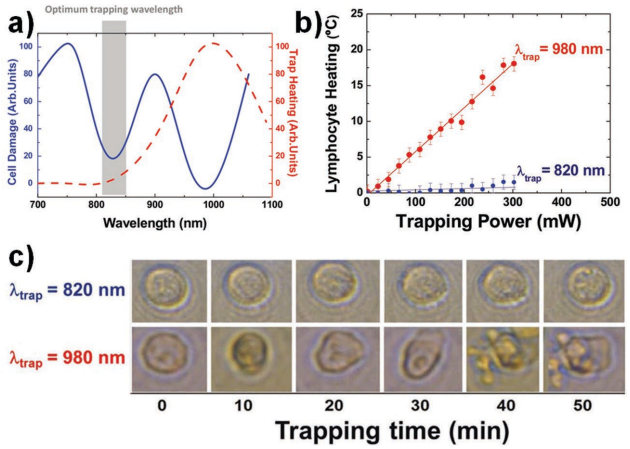

Figure 18. Thermal spectroscopy and imaging of optically trapped microspheres and single cells using QDs. a) The wavelength dependence of laser-induced CHO (Chinese Hamster Ovary) cell damage after optical trapping (solid line), and the wavelength dependence of the laser-induced thermal loading of an optical trap (dashed line). b) Intracellular temperature increment produced in the trapped lymphocyte as a function of the trapping laser obtained at two different wavelengths (820 and 980 nm). c) Optical transmission images of a single trapped lymphocyte as obtained for different trapping durations. Reproduced with permission.[48] Copyright 2013, Wiley-VCH.

successfully realizes the thermal contact. The reproducibility (>99.5%), the fast time response, and the high temperature sensitivity (5.8%/°C) in the physiological temperature range (22–42 °C) ensure a good performance in thermosensing of living cells. After the incubation of heater/thermometer NPs with opossum kidney (OK) cells, fluorescence images showed the internalization of these NPs, mostly around the nucleus, which enables the thermometric mapping at subcellular scale by simply taking the pixel-by-pixel ratio of the Eu^{3+}/Tb^{3+} intensities.

6. Conclusion and Future Perspectives

Over the past decade, multifarious thermometers for intracellular temperature detection have been developed and the number of works is on the increase in recent years. This young and active area indicates a great demand of cellular thermometry in fundamental research of cytobiology and clinical treatment of diseases. While these techniques have been able to accomplish this goal basically, they still stay in the experimental stage due to some drawbacks. Few studies have been conducted to further survey the mechanism of activity-related cellular thermogenesis. The thermocouple has a high temperature resolution, fast response and large detection range, but it often compromises the cell's integrity in measurement. Organic fluorophores are unqualified for continuous longtime detection limited by photobleaching and pH sensitivity. Apart from the instability and toxicity under intracellular acidic environment with different ionic strength, the size and shape distribution of QDs results in a non-homogeneous luminescence. Fluorescent polymetric thermometers have a slow response due to the hysteretic phase transitions. Biomolecule-based thermometers are complicated and cumbersome, and should be calibrated to selectively and frequently. What's more, in some systems, the thermometers are multi-parameter sensitive (pH, ionic strength, solution viscosity and so on), which makes the precise determination of temperature difficult. Systematic and comprehensive calibration in solutions with different pH or ion strength, cell extracts and in living cell's internal, is essential to deal with this problem. However, the development of the thermometer only sensitive to temperature would be more effective.

To date, all cellular thermometry are in urgent need of universal reference standards and theoretical calculation based on math-physical model to guarantee the accuracy of the signal measured in living cells.[1,117–120] In the theoretical work of Baffou et al., they argued that a single cell cannot substantially raise its temperature by endogenous thermogenesis.[117] The measured temperature increase of 1–2 K in a single cell using cellular thermometry is much larger than the theoretically calculated increase limit of 10^{-5} K. However, other researchers did not believe that all the results measured by completely different kinds of thermometers are due to some factors else instead of temperature changes, and thought that Baffou's theoretical model was not suitable for a real cell.[118,119] A more accurate referential thermometer and a comprehensive theoretical model are greatly required for the existing cellular thermometers to prove their validity. Combining two different thermometers together into one probe may be simple and direct validation method. In addition, from the kinetic molecular theory's point of view, temperature is essentially a number that is directly proportional to the average kinetic energy of the molecules in a substance. Thus, the fluctuations of a Brownian particle can be used to ascertain the properties of its environment.[121] Analyzing the nanosphere's Brownian motion offers an opportunity for more direct and accurate temperature measurements with spatial resolution on the nanoscale, which has important value of reference to cellular thermometry.[121,122] Summarily, cellular thermometry is still in its childhood and already provides promising outlooks. With its ongoing progress, it is undoubtedly that cellular thermometry would be a powerful tool and greatly contribute to the development of cytobiology or life science.

Acknowledgements

The authors acknowledge the financial support from the National Key Basic Research Program of China (2013CB733804), the National Natural Science Foundation of China for Key Project of International Cooperation (61420106012), and the Special Project on Development of National Key Scientific Instruments Equipment of China (2011YQ03013403).

[1] U. Lucia, G. Grazzini, B. Montrucchio, G. Grisolia, R. Borchiellini, G. Gervino, C. Castagnoli, A. Ponzetto, F. Silvagno, *Sci. Rep.* **2015**, *5*, 11587.

[2] P. J. Stoward, *Nature* **1962**, *194*, 977.
[3] G. N. Somero, *Annu. Rev. Physiol.* **1995**, *57*, 43.
[4] L. Carlos, *Thermometry at the Nanoscale: Techniques and Selected Applications*, Royal Society of Chemistry, **2015**.
[5] S. A. Binslem, M. R. Ahmad, Z. Awang, *J. Teknologi* **2015**, *73*, 71.
[6] R. Sakaguchi, S. Kiyonaka, Y. Mori, *Curr. Opin. Biotechnol.* **2015**, *31*, 57.
[7] D. Jaque, B. d. Rosal, E. M. Rodríguez, L. M. Maestro, P. Haro-González, J. G. Solé, *Nanomedicine* **2014**, *9*, 1047.
[8] B. Alberts, D. Bray, K. Hopkin, A. Johnson, J. Lewis, M. Raff, K. Roberts, P. Walter, *Essential Cell Biology*, Garland Science, **2013**.
[9] F. E. Stockdale, H. Holtzer, *Exp. Cell Res.* **1961**, *24*, 508.
[10] R. Sitia, I. Braakman, *Nature* **2003**, *426*, 891.
[11] M. Yoshida, E. Muneyuki, T. Hisabori, *Nat. Rev. Mol. Cell Biol.* **2001**, *2*, 669.
[12] J. S. Donner, S. A. Thompson, C. s. Alonso-Ortega, J. Morales, L. G. Rico, S. I. O. Santos, R. Quidant, *ACS Nano* **2013**, *7*, 8666.
[13] B. B. Lowell, B. M. Spiegelman, *Nature* **2000**, *404*, 652.
[14] J. Himms-Hagen, *Annu. Rev. Physiol.* **1976**, *38*, 315.
[15] E. Tanaka, M. Yamamura, A. Yamakawa, T. Fujise, S. Nakano, *Biochem. Int.* **1992**, *26*, 873.
[16] G. V. Gavriloaia, A. Hurduc, A. M. Ghimigean, R. Fumarel, *Proc SPIE* **2009**.
[17] C. Gota, K. Okabe, T. Funatsu, Y. Harada, S. Uchiyama, *J. Am. Chem. Soc.* **2009**, *131*, 2766.
[18] P. Wust, B. Hildebrandt, G. Sreenivasa, B. Rau, J. Gellermann, H. Riess, R. Felix, P. M. Schlag, *Lancet Oncol.* **2002**, *3*, 487.
[19] B. Hildebrandt, P. Wust, O. Ahlers, A. Dieing, G. Sreenivasa, T. Kerner, R. Felix, H. Riess, *Crit. Rev. Oncol. Hematol.* **2002**, *43*, 33.
[20] D. Moreau, C. Lefort, R. Burke, P. Leveque, R. P. O'Connor, *Biomed. Opt. Express* **2015**, *6*, 4105.
[21] L. M. Maestro, P. Haro-González, B. Del Rosal, J. Ramiro, A. Caamano, E. Carrasco, A. Juarranz, F. Sanz-Rodríguez, J. G. Solé, D. Jaque, *Nanoscale* **2013**, *5*, 7882.
[22] Y. Feng, Z. f. Luo, S. S. Qu, C. Y. Zeng, H. Xu, *Thermochim. Acta* **1997**, *303*, 203.
[23] M. Monti, I. Wadsö, *Acta Med. Scand.* **1976**, *200*, 301.
[24] L. E. Erickson, In A. M. James Ed: *Thermal and Energetic Studies of Cellular Biological Systems*, IOP Publishing Ltd., Bristol, **1987**, 14.
[25] K. Levin, P. Furst, R. Harris, E. Hultman, *Scand. J. Clin. Lab. Invest.* **1974**, *34*, 141.
[26] A. Waldenström, I. Engström, G. Ronquist, *J. Intern. Med.* **2001**, *249*, 97.
[27] I. Engström, A. Waldenström, P. Nilsson-Ehle, G. Ronquist, *Clin. Chim. Acta* **1993**, *219*, 113.
[28] H. Böttcher, P. Fürst, *Baillieres Clin. Endocrinol. Metab.* **1997**, *11*, 739.
[29] Y. Wang, G. Holroyd, A. M. Hetherington, C. K. Y. Ng, *J. Exp. Bot.* **2004**, *55*, 1187.
[30] M. A. Paulik, R. G. Buckholz, M. E. Lancaster, W. S. Dallas, E. A. Hull-Ryde, J. E. Weiel, J. M. Lenhard, *Pharm. Res.* **1998**, *15*, 944.
[31] X.-d. Wang, O. S. Wolfbeis, R. J. Meier, *Chem. Soc. Rev.* **2013**, *42*, 7834.
[32] C. D. S. Brites, P. P. Lima, N. J. O. Silva, A. Millan, V. S. Amaral, F. Palacio, L. D. Carlos, *Nanoscale* **2012**, *4*, 4799.
[33] D. Jaque, F. Vetrone, *Nanoscale* **2012**, *4*, 4301.
[34] H. Zhou, M. Sharma, O. Berezin, D. Zuckerman, M. Y. Berezin, *ChemPhysChem* **2015**, *17*, 27.
[35] C. F. Chapman, Y. Liu, G. J. Sonek, B. J. Tromberg, *Photochem. Photobiol.* **1995**, *62*, 416.
[36] H. Huang, S. Delikanli, H. Zeng, D. M. Ferkey, A. Pralle, *Nat. Nanotechnol.* **2010**, *5*, 602.
[37] S. Arai, S.-C. Lee, D. Zhai, M. Suzuki, Y. T. Chang, *Sci. Rep.* **2014**, *4*, 6701.
[38] H. Itoh, S. Arai, T. Sudhaharan, S.-C. Lee, Y.-T. Chang, S. i. Ishiwata, M. Suzuki, E. B. Lane, *Chem. Commun.* **2016**, *52*, 4458.
[39] S. Arai, M. Suzuki, S.-J. Park, J. S. Yoo, L. Wang, N.-Y. Kang, H.-H. Ha, Y.-T. Chang, *Chem. Commun.* **2015**, *51*, 8044.
[40] M. Homma, Y. Takei, A. Murata, T. Inoue, S. Takeoka, *Chem. Commun.* **2015**, *51*, 6194.
[41] O. Zohar, M. Ikeda, H. Shinagawa, H. Inoue, H. Nakamura, D. Elbaum, D. L. Alkon, T. Yoshioka, *Biophys. J.* **1998**, *74*, 82.
[42] M. Suzuki, V. Tseeb, K. Oyama, S. Ishiwata, *Biophys. J.* **2007**, *92*, L46.
[43] K. Oyama, M. Takabayashi, Y. Takei, S. Arai, S. Takeoka, S. Ishiwata, M. Suzuki, *Lab Chip* **2012**, *12*, 1591.
[44] L. Yang, H.-S. Peng, H. Ding, F.-T. You, L.-L. Hou, F. Teng, *Microchim. Acta* **2014**, *181*, 743.
[45] L. M. Maestro, E. M. Rodriguez, F. S. Rodriguez, M. C. la Cruz, A. Juarranz, R. Naccache, F. Vetrone, D. Jaque, J. A. Capobianco, J. G. Sole, *Nano Lett.* **2010**, *10*, 5109.
[46] L. M. Maestro, P. Haro-González, M. C. Iglesias-De La Cruz, F. SanzRodríguez, Á. Juarranz, J. G. Solé, D. Jaque, *Nanomedicine* **2013**, *8*, 379.
[47] J. M. Yang, H. Yang, L. Lin, *ACS Nano* **2011**, *5*, 5067.
[48] P. Haro-González, W. T. Ramsay, L. M. Maestro, B. del Rosal, K. Santacruz-Gomez, F. Sanz-Rodríguez, J. Y. Chooi, P. R. Sevilla, M. Bettinelli, D. Choudhury, *Small* **2013**, *9*, 2162.
[49] H. Liu, Y. Fan, J. Wang, Z. Song, H. Shi, R. Han, Y. Sha, Y. Jiang, *Sci. Rep.* **2015**, *5*, 14879.
[50] F. Vetrone, R. Naccache, A. Zamarrón, A. J. de la Fuente, F. Sanz-Rodríguez, L. M. Maestro, E. M. Rodriguez, D. Jaque, J. G. Solé, J. A. Capobianco, *ACS Nano* **2010**, *4*, 3254.
[51] U. Rocha, C. J. da Silva, W. F. Silva, I. Guedes, A. Benayas, L. M. Maestro, M. A. Elias, E. Bovero, F. C. J. M. van Veggel, J. A. G. Solé, D. Jaque, *ACS Nano* **2013**, *7*, 1188.
[52] P. Rodríguez-Sevilla, Y. Zhang, P. Haro-González, F. Sanz-Rodríguez, F. Jaque, J. G. Solé, X. Liu, D. Jaque, *Adv. Mater.* **2016**, *28*, 2421.
[53] L. Shang, F. Stockmar, N. Azadfar, G. U. Nienhaus, *Angew. Chem. Int. Ed. Engl.* **2013**, *52*, 11154.
[54] G. Kucsko, P. Maurer, N. Yao, M. Kubo, H. Noh, P. Lo, H. Park, M. Lukin, *Nature* **2013**, *500*, 54.
[55] C. Wang, L. Ling, Y. Yao, Q. Song, *Nano Res.* **2015**, *8*, 1975.
[56] J. Qiao, L. Qi, Y. Shen, L. Zhao, C. Qi, D. Shangguan, L. Mao, Y. Chen, *J. Mater. Chem.* **2012**, *22*, 11543.
[57] K. Okabe, N. Inada, C. Gota, Y. Harada, T. Funatsu, S. Uchiyama, *Nat. Commun.* **2012**, *3*, 705.
[58] T. Tsuji, S. Yoshida, A. Yoshida, S. Uchiyama, *Anal. Chem.* **2013**, *85*, 9815.
[59] T. Hayashi, N. Fukuda, S. Uchiyama, N. Inada, *PLoS ONE* **2015**, *10*, e0117677.
[60] Z. Wang, X. Ma, S. Zong, Y. Wang, H. Chen, Y. Cui, *Talanta* **2015**, *131*, 259.
[61] J. S. Donner, S. A. Thompson, M. P. Kreuzer, G. Baffou, R. Quidant, *Nano Lett.* **2012**, *12*, 2107.
[62] S. Kiyonaka, T. Kajimoto, R. Sakaguchi, D. Shinmi, M. Omatsu-Kanbe, H. Matsuura, H. Imamura, T. Yoshizaki, I. Hamachi, T. Morii, *Nat. Methods* **2013**, *10*, 1232.
[63] G. Ke, C. Wang, Y. Ge, N. Zheng, Z. Zhu, C. J. Yang, *J. Am. Chem. Soc.* **2012**, *134*, 18908.
[64] C. Wang, R. Xu, W. Tian, X. Jiang, Z. Cui, M. Wang, H. Sun, K. Fang, N. Gu, *Cell Res.* **2011**, *21*, 1517.
[65] R. Shrestha, T. Y. Choi, W. Chang, D. Kim, *Sensors-Basel* **2011**, *11*, 8826.

DOI: 10.1002/smll.201600665

[66] S. Herth, M. Giesguth, W. Wedel, G. Reiss, K.-J. Dietz, *Appl. Phys. Lett.* **2013**, *102*, 103505.
[67] S. A. Binslem, M. R. Ahmad, *J. Teknologi* **2014**, *70*, 81.
[68] F. Li, A. H. Westphal, A. T. M. Marcelis, E. J. R. Sudholter, M. A. Cohen Stuart, F. A. M. Leermakers, *Soft Matter* **2011**, *7*, 11211.
[69] A. E. Albers, E. M. Chan, P. M. McBride, C. M. Ajo-Franklin, B. E. Cohen, B. A. Helms, *J. Am. Chem. Soc.* **2012**, *134*, 9565.
[70] J. Qiao, C. Chen, L. Qi, M. Liu, P. Dong, Q. Jiang, X. Yang, X. Mu, L. Mao, *J. Mater. Chem. B* **2014**, *2*, 7544.
[71] Y. Takei, S. Arai, A. Murata, M. Takabayashi, K. Oyama, S. i. Ishiwata, S. Takeoka, M. Suzuki, *ACS Nano* **2014**, *8*, 198.
[72] R. Piñol, C. D. S. Brites, R. Bustamante, A. Martínez, N. J. O. Silva, J. L. Murillo, R. Cases, J. Carrey, C. Estepa, C. Sosa, F. Palacio, L. D. Carlos, A. Millán, *ACS Nano* **2015**, *9*, 3134.
[73] S. Arai, Ferdinandus, S. Takeoka, S. i. Ishiwata, H. Sato, M. Suzuki, *Analyst* **2015**, *140*, 7534.
[74] E. N. Cerón, D. H. Ortgies, B. del Rosal, F. Ren, A. Benayas, F. Vetrone, D. Ma, F. Sanz-Rodríguez, J. G. Solé, D. Jaque, *Adv. Mater.* **2015**, *27*, 4781.
[75] J. Liu, X. Guo, R. Hu, J. Xu, S. Wang, S. Li, Y. Li, G. Yang, *Anal. Chem.* **2015**, *87*, 3694.
[76] S. Uchiyama, T. Tsuji, K. Ikado, A. Yoshida, K. Kawamoto, T. Hayashi, N. Inada, *Analyst* **2015**, *140*, 4498.
[77] J. Qiao, Y.-H. Hwang, C.-F. Chen, L. Qi, P. Dong, X.-Y. Mu, D.-P. Kim, *Anal. Chem.* **2015**, *87*, 10535.
[78] X. Hu, Y. Li, T. Liu, G. Zhang, S. Liu, *ACS Appl. Mater. Interfaces* **2015**, *7*, 15551.
[79] D. Ross, M. Gaitan, L. E. Locascio, *Anal. Chem* **2001**, *73*, 4117.
[80] J. Gallery, M. Gouterman, J. Callis, G. Khalil, B. McLachlan, J. Bell, *Rev. Sci. Instrum.* **1994**, *65*, 712.
[81] N. C. Bal, S. K. Maurya, D. H. Sopariwala, S. K. Sahoo, S. C. Gupta, S. A. Shaikh, M. Pant, L. A. Rowland, S. A. Goonasekera, J. D. Molkentin, M. Periasamy, *Nat. Med.* **2012**, *18*, 1575.
[82] M. L. Bhaumik, *J. Chem. Phys.* **1964**, *40*, 3711.
[83] H. Peng, M. I. J. Stich, J. Yu, L.-n. Sun, L. H. Fischer, O. S. Wolfbeis, *Adv. Mater.* **2010**, *22*, 716.
[84] A. J. Morgan, R. Jacob, *Biochem. J.* **1994**, *300*, 665.
[85] J. Van Houten, R. J. Watts, *J. Am. Chem. Soc.* **1976**, *98*, 4853.
[86] J. Lee, N. A. Kotov, *Nano Today* **2007**, *2*, 48.
[87] G. W. Walker, V. C. Sundar, C. M. Rudzinski, A. W. Wun, M. G. Bawendi, D. G. Nocera, *Appl. Phys. Lett.* **2003**, *83*, 3555.
[88] A. M. Smith, H. W. Duan, A. M. Mohs, S. M. Nie, *Adv. Drug Delivery Rev.* **2008**, *60*, 1226.
[89] S. Li, K. Zhang, J. M. Yang, L. Lin, H. Yang, *Nano Lett.* **2007**, *7*, 3102.
[90] J. M. Yang, H. Yang, L. Lin, *2010 IEEE 23rd Conference on Micro Electro Mechanical Systems (MEMS)*, Hong Kong, China, **2010**.
[91] D. Zhou, M. Lin, X. Liu, J. Li, Z. Chen, D. Yao, H. Sun, H. Zhang, B. Yang, *ACS Nano* **2013**, *7*, 2273.
[92] P. T. C. So, C. Y. Dong, B. R. Masters, K. M. Berland, *Annu. Rev. Biomed. Eng.* **2000**, *2*, 399.
[93] C. Xu, W. Zipfel, J. B. Shear, R. M. Williams, W. W. Webb, *Proc. Natl. Acad. Sci. USA* **1996**, *93*, 10763.
[94] Z. Li, Y. Zhang, H. La, R. Zhu, G. El-Banna, Y. Wei, G. Han, *Nanomaterials-Basel* **2015**, *5*, 2148.
[95] X. Chen, J. B. Essner, G. A. Baker, *Nanoscale* **2014**, *6*, 9594.
[96] H. Huang, H. Li, A.-J. Wang, S.-X. Zhong, K.-M. Fang, J.-J. Feng, *Analyst* **2014**, *139*, 6536.
[97] P. Neumann, I. Jakobi, F. Dolde, C. Burk, R. Reuter, G. Waldherr, J. Honert, T. Wolf, A. Brunner, J. H. Shim, *Nano Lett.* **2013**, *13*, 2738.
[98] D. M. Toyli, C. F. de las Casas, D. J. Christle, V. V. Dobrovitski, D. D. Awschalom, *Proc. Natl. Acad. Sci. USA* **2013**, *110*, 8417.
[99] M. A. Zurbuchen, M. P. Lake, S. A. Kohan, B. Leung, L.-S. Bouchard, *Sci. Rep.* **2013**, *3*, 2668.
[100] C. Sealy, *Nanotoday* **2013**, *8*, 451.
[101] K. Sokolov, *Nature* **2013**, *500*, 36.
[102] S. Ebrahimi, Y. Akhlaghi, M. Kompany-Zareh, Å. Rinnan, *ACS Nano* **2014**, *8*, 10372.
[103] K. Kim, W. Jeong, W. Lee, P. Reddy, *ACS Nano* **2012**, *6*, 4248.
[104] M. Watanabe, N. Kakuta, K. Mabuchi, Y. Yamada, in *Proceedings of 27th Annual International Conference of the Engineering in Medicine, Biology Society*, IEEE-EMBS*2005*, Shanghai, China, **2005**, *5*, 4858.
[105] R. Shrestha, T. Y. Choi, W. S. Chang, *SENSORS 2010,* IEEE, Kona, Hawaii, **2010**.
[106] T. Wenjuan, W. Cangling, W. Jianqing, C. Qiuhua, S. Jianfei, L. Can, W. Xing, G. Ning, *Nanotechnology* **2015**, *26*, 355501.
[107] N. Inomata, M. Toda, M. Sato, A. Ishijima, T. Ono, *Appl. Phys. Lett.* **2012**, *100*, 154104.
[108] C. Y. Chen, C. T. Chen, *Chem. Commun.* **2011**, *47*, 994.
[109] L. Song, E. J. Hennink, I. T. Young, H. J. Tanke, *Biophys. J.* **1995**, *68*, 2588.
[110] A. R. Bayles, H. S. Chahal, D. S. Chahal, C. P. Goldbeck, B. E. Cohen, B. A. Helms, *Nano Lett.* **2010**, *10*, 4086.
[111] H. Mattoussi, G. Palui, H. B. Na, *Adv. Drug Delivery Rev.* **2012**, *64*, 138.
[112] P. M. Bendix, S. N. S. Reihani, L. B. Oddershede, *ACS Nano* **2010**, *4*, 2256.
[113] C. Li, X. Gan, X. Li, M. Gu, *Appl. Phys. Lett.* **2015**, *107*, 121105.
[114] M. L. Debasu, D. Ananias, I. Pastoriza-Santos, L. M. Liz-Marzán, J. Rocha, L. D. Carlos, *Adv. Mater.* **2013**, *25*, 4868.
[115] S. Freddi, L. Sironi, R. D'Antuono, D. Morone, A. Donà, E. Cabrini, L. D'Alfonso, M. Collini, P. Pallavicini, G. Baldi, *Nano Lett.* **2013**, *13*, 2004.
[116] J. Dong, J. I. Zink, *ACS Nano* **2014**, *8*, 5199.
[117] G. Baffou, H. Rigneault, D. Marguet, L. Jullien, *Nat. Methods* **2014**, *11*, 899.
[118] S. Kiyonaka, R. Sakaguchi, I. Hamachi, T. Morii, T. Yoshizaki, Y. Mori, *Nat. Methods* **2015**, *12*, 801.
[119] M. Suzuki, V. Zeeb, S. Arai, K. Oyama, S. i. Ishiwata, *Nat. Methods* **2015**, *12*, 802.
[120] G. Baffou, H. Rigneault, D. Marguet, L. Jullien, *Nat. Methods* **2015**, *12*, 803.
[121] J. Millen, T. Deesuwan, P. Barker, J. Anders, *Nat. Nanotechnol.* **2014**, *9*, 425.
[122] K. Kroy, *Nat. Nanotechnol.* **2014**, *9*, 415.

Received: February 28, 2016
Revised: March 28, 2016
Published online: